

Co-Designing Statistical MIMO Radar and In-band Full-Duplex Multi-User MIMO Communications

Jiawei Liu, *Student Member IEEE*, Kumar Vijay Mishra, *Senior Member IEEE*,
and Mohammad Saquib, *Senior Member IEEE*

Abstract—We present a spectral co-design of a statistical multiple-input-multiple-output (MIMO) radar and an in-band full-duplex (IBFD) multi-user MIMO (MU-MIMO) communications system both of which concurrently operate within the same frequency band. Prior works on MIMO-radar-MIMO-communications (MRMC) problem either focus on colocated MIMO radars and half-duplex/single-user MIMO communications, seek coexistence solutions, do not jointly design waveforms and receiver processing or omit practical system constraints. Here, we jointly design statistical MIMO radar waveform, uplink (UL)/downlink (DL) precoders, and receive filters. To this end, we employ a novel performance measure, namely compounded-and-weighted sum mutual information (CWSM), that is subjected to multiple practical constraints of UL/DL transmit power, UL/DL quality of service, and peak-to-average-power-ratio. We solve the resulting non-convex problem by incorporating block coordinate descent (BCD) and alternating projection (AP) methods in a single algorithmic framework called BCD-AP MRMC. We achieve this by exploiting the relationship between mutual information and weighted minimum mean-squared-error (WMMSE), which allows use of the Lagrange dual problem in finding closed-form solutions for precoders and radar waveform. Numerical experiments show that our proposed WMMSE-based method quickly achieves monotonic convergence, improves target detection by 6-13% compared to conventional radar coding, and provides 8.3-30% higher rate in IBFD MU-MIMO system than other precoding strategies.

Index Terms—Alternating projection, block coordinate descent, in-band full-duplex MU MIMO, MIMO radar, WMMSE.

I. INTRODUCTION

Severe crowding of the electromagnetic spectrum in recent years has led to complex challenges in designing radar and communications systems that operate in the same bands [1]. Both systems need a wide bandwidth to provide a designated quality-of-service (QoS) [2]. Whereas a high-resolution detection of radar targets requires large transmit signal bandwidths, the wireless cellular networks need access to wide spectrum to support high data rates [3]. The continuous scaling up of the carrier frequencies and deployment of wireless communications has led the spectrum regulators to allow use of the spectrum traditionally reserved for the radar (sensing) applications for commercial communications systems. As a result, many concerted spectrum-sharing efforts are underway to design new sensing and processing modalities for radar and communications [1].

In [4], a comprehensive taxonomy of different design philosophies to achieve the coexistence of radar and communications systems was summarized. Broadly, the two most common approaches are sharing with spectral overlap (or *coexistence*) and functional spectrum-sharing (or *co-design*). In the former, both systems have separate units that operate within the same spectrum using different waveforms. The latter combines the two systems at either transmitter (Tx), receiver (Rx) or both in a single hardware platform and employs a common waveform [1, 5, 6]. These spectrum-sharing solutions also depend on the level of cooperation between radar and communications. In a *selfish* paradigm, the overall architecture usually promotes the performance of only one system leading to radar-centric [7–9] and

communications-centric [10] coexistence solutions. On the other hand, the *holistic* solution relies on extensive mutual cooperation between the two systems in terms of transmit strategies and receive processing [3, 11–16]. The exchange of information, such as the channel state information (CSI), may also be facilitated through a fusion center [12, 16]. The spectral cooperation not only enables both systems to benefit from an increased number of degrees-of-freedom (DoFs) but also allows joint optimization of system parameters through one [12, 13] or more [3, 17] objective functions. For example, the communications signals decoded at the radar Rx may be used to enhance target detection/localization [3, 16]. Similarly, communications Rx may improve error rates by also extracting symbols embedded in the echoes reflected off the radar targets [18]. In this paper, we focus on this holistic spectral co-design.

These approaches do not easily extend [17, 19] to multiple-input multiple-output (MIMO) configuration, which employs several Tx and Rx antennas to achieve high spectrum efficiency [20, 21]. In communications, MIMO configuration enhances capacity, provides spatial diversity, and exploits multipath propagation [20]. Further, recent developments in massive MIMO [22] have demonstrated that uplink/downlink (UL/DL) channel reciprocity can be exploited by deploying very large number of service antennas to serve a lower number of mobile users with the time-division-duplexing.

Similarly, MIMO radars outweigh an equivalent, standard phased array radar by offering higher angular resolution with fewer antennas, spatial diversity, and improved parameter identifiability by exploiting waveform diversity [21]. In a *colocated* MIMO radar [23, 24], the radar cross-section (RCS) is identical to closely-spaced antennas. On the contrary, the antennas in a *widely distributed* MIMO radar are sufficiently separated from each other such that the same target projects a different RCS to each Tx-Rx pair; this spatial diversity is advantageous in detecting targets with small backscatter and low speed [25, 26]. The distributed system is also called *statistical* MIMO radar because the path gain vectors in a distributed array are modeled as independent statistical variables [25–28].

The increased DoFs, sharing of antennas, and higher dimensional optimization exacerbate spectrum sharing in a joint MIMO-radar-MIMO-communications (MRMC) architecture [17, 19]. Early works on MRMC proposed null space projection (NSP) beamforming which projects the colocated MIMO radar signals onto the nullspace of the interference channel matrix from radar Tx to MIMO communications Rx [29]. The MRMC processing techniques included matrix completion [12], single base station (BS) interference mitigation [29], and switched small singular value space projection [11]. Among waveforms, [8] analyzed orthogonal frequency-division multiplexing (OFDM) for MIMO radar to coexist with a communications system. On the other hand, [13, 14] suggest optimal space-time transmit waveforms for a colocated MIMO radar that is jointly designed with point-to-point (P2P) MIMO communications codebook.

Nearly all of these works focus on single-user (SU) MIMO communications and colocated MIMO radars. In order to generalize MRMC, [18] investigated a novel constructive-interference-based precoding optimization for colocated MIMO radar and DL MU multiple input single-output (MISO) communications. This was later extended to coexistence of MIMO radar with MU-MIMO communications [5]

J. L. and M. S. are with the Department of Electrical and Computer Engineering, The University of Texas at Dallas, Richardson Tx, 75080 USA. E-mail: {jiawei.liu3, saquib}@utdallas.edu.

K. V. M. is with the United States Army Research Laboratory, Adelphi MD, 20783 USA. E-mail: kumarvijay-mishra@uiowa.edu.

through multiple radar transmit beamforming approaches that keep the original modulation and communications data rate unaffected. In quite a few recent studies [4, 30], either radar and communications is in MIMO configuration.

Co-design with statistical MIMO radar remains relatively unexamined in these prior works. Whereas the model in [16] comprises widely distributed MIMO radar, it studies coexistence with a simplistic P2P MIMO communications. Note that even the MIMO communications considered in aforementioned works usually avoid a joint UL-DL design and focus on only one of them. These studies also sidestep investigations of full-duplex (FD) mode, even though it is critical for fifth-generation (5G) wireless networks. In particular, in-band FD (IBFD) MIMO communications allows UL and DL to function on the same frequency band simultaneously, thereby doubling the throughput of a traditional MIMO cellular system [31]. This challenging mode is successful only if the transmit signal is suppressed below acceptable levels to prevent the receive chain saturation. The BS used in the MRMC design of [3] operates in MU FD mode and serves multiple DL and UL users simultaneously using identical bandwidth and transmission times. However, the design philosophy is that of coexistence with a colocated MIMO radar.

In this work, we address these gaps by proposing a co-design for a statistical MIMO radar and IBFD MU-MIMO communications system. As in most IBFD MU-MIMO systems [3, 31, 32], we assume that BSs operate in FD while DL or UL user equipment (UE) in half-duplex (HD) mode. Further, unlike many prior works that focus on only one specific system goal and often in isolation with other processing modules, we jointly design the UL/DL precoders, MIMO radar waveform matrix, and linear receive filters (LRFs) for both systems. Our novel approach exploits mutual information (MI) by proposing a novel *compounded-and-weighted sum MI* (CWSM) to measure the combined performance of the radar and communications systems. When compared with similar MI-based studies in [3, 16, 32] that adopt different metrics for radar and communications, the CWSM is reflective of the performance of both systems.

Our co-design also accounts for several practical constraints including maximum UL/DL transmit power, QoS of the UL/DL quantified by their respective minimum achievable rates, and peak-to-average-power-ratio (PAR) of the MIMO radar waveform. Note that, despite the operational importance of PAR in MIMO radar waveform design, it has been rarely accounted for in earlier MRMC literature. To address the challenges imposed by the non-convex CWSM maximization problem with several constraints, we develop an alternating algorithm that incorporates both block coordinate descent (BCD) and alternating projection (AP) methods. This BCD-AP MRMC method breaks the original problem to less complex subproblems that are then iteratively solved. Numerical experiments show quick, monotonic convergence of our proposed algorithm. Using our optimized radar codes, the target detection is enhanced up to 13% over conventional radar waveforms at a given false alarm rate. Our optimized precoders yield up to 30% higher rate than standard precoders.

The remainder of the paper is organized as follows. In the next section, we describe the system models of the statistical MIMO radar and the IBFD-MIMO communications system, respectively. In Section III, we formulate the co-design problem as a CWSM maximization. We then present our BCD-AP MRMC procedure to solve the optimization problem iteratively in Section IV. Finally, we validate our proposed technique through numerical experiments in Section V. We conclude in Section VI.

Notation: lowercase and uppercase letters in bold denote columns and matrices, respectively, and lowercase letters in italics represent scalars. We use $I(\mathbf{X}; \mathbf{Y})$ and $H(\mathbf{X}|\mathbf{Y})$ to denote, respectively, MI and conditional entropy between two random variables \mathbf{X} and

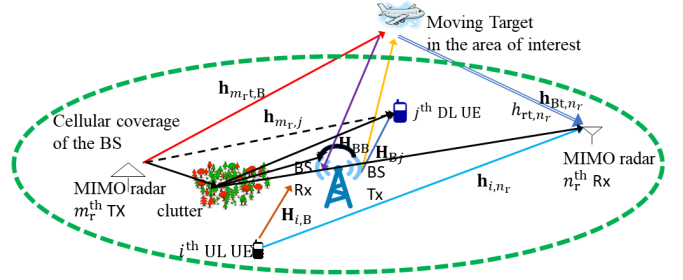


Fig. 1. Co-design system model comprising a statistical (widely distributed) MIMO radar and IBFD MU-MIMO communications.

\mathbf{Y} . The notation $\mathbf{Y}[k]$, $\mathbf{y}[k]$, and $y[k]$ denote the value of time-variant matrix \mathbf{Y} , vector \mathbf{y} and scalar y at discrete time index k , respectively; $\mathbf{1}_N$ is a vector of size N with all ones; and \mathbb{C} and \mathbb{R} represent sets of complex and real numbers, respectively; a circularly symmetric complex Gaussian (CSCG) vector \mathbf{q} with N elements and power spectral density \mathcal{N}_0 is $\mathbf{q} \sim \mathcal{CN}(0, \mathcal{N}_0 \mathbf{I}_N)$; $\mathbb{E}[\cdot]$ is the statistical expectation; $\text{Tr}\{\mathbf{R}\}$, \mathbf{R}^\top , \mathbf{R}^\dagger , $|\mathbf{R}|$, $\mathbf{R} \succeq \mathbf{0}$, and $\mathbf{R}(m, n)$ are the trace, transpose, Hermitian transpose, determinant, positive semi-definiteness and (m, n) th entry of matrix \mathbf{R} , respectively; and set $\mathbb{Z}_+(L)$, $\mathbf{x} \succeq \mathbf{y}$, x^+ , $x^{(t)}(\cdot)$, \inf and \oplus denote $\{1, \dots, L\}$, component-wise inequality between vectors \mathbf{x} and \mathbf{y} , $\max(x, 0)$, the t th iterate of an iterative function $x(\cdot)$, infimum, and direct sum, respectively.

II. SPECTRAL CO-DESIGN SYSTEM MODEL

Consider a statistical MIMO radar whose goal is to detect a moving target in a region that is coterminous with the cellular coverage of a BS which receives data from I UL UEs while transmit it to J DL UEs (Fig. 1) The M_r Tx and N_r Rx of the statistical MIMO radar are located in a 2-D plane (x, y) along with the BS, the I UL UEs and the J DL UEs at coordinates (x_{m_r}, y_{m_r}) , $m_r \in \mathbb{Z}_+(M_r)$ and (x_{n_r}, y_{n_r}) , $n_r \in \mathbb{Z}_+(N_r)$, (x_B, y_B) , (x_{n_i}, y_{n_i}) , and (x_{n_j}, y_{n_j}) , $n \in \mathbb{Z}_+(N)$, respectively. In the sequel, we describe the system models of each of these units in detail and then present the co-design formulation.

A. Statistical MIMO Radar System

Each radar Tx emits a pulse train of K pulses at a pulse repetition interval (PRI) of T_r toward targets-of-interest; this yields a *coherent processing interval* (CPI) of $K T_r$. The pulse train corresponding to the m_r th Tx is modulated by the waveform code $\mathbf{a}_{m_r} \in \mathbb{C}^K$ and the MIMO radar code matrix is $\mathbf{A} = [\mathbf{a}^\top[1]; \dots; \mathbf{a}^\top[K]] \in \mathbb{C}^{K \times M_r}$, where $\mathbf{a}[k] = [a_1[k], \dots, a_{M_r}[k]]^\top$ is a radar code vector transmitted during the k th PRI. Each pulse duration is $T_P = T_r/N$, where $N \in \mathbb{Z}$ denotes the number of range cells/samples in a single PRI. The pulse train emitted by the m_r th Tx is

$$s_{m_r}(t) = \sum_{k=1}^K a_{m_r,k} \phi_{m_r}(t - (k-1)T_r), \quad (1)$$

where $\phi_{m_r}(t)$ denotes the m_r th element of the narrowband transmit waveform vector $\boldsymbol{\phi}(t) = [\phi_1(t), \dots, \phi_{M_r}(t)]^\top$ that satisfies the orthonormality condition $\int_{T_P} \boldsymbol{\phi}(t) \boldsymbol{\phi}^\dagger(t) dt = \mathbf{I}_{M_r}$. The transmit signal of all Tx are $\mathbf{s}(t) = [s_1(t), \dots, s_{M_r}(t)]^\top$.

We consider a near-field scenario where the target scenario has an extended target composed of a large number of independent point-like scatterers. The complex reflectivity of the extended target corresponding to the m_r th Tx - n_r th Rx link $h_{m_r n_r}$ is modeled as a CSCG random variable $h_{m_r n_r} \sim \mathcal{CN}(0, \eta_{m_r n_r}^2)$, where $\eta_{m_r n_r}^2$ denotes the average reflection power of the extended target; it remains constant over the CPI as per the Swerling I (block fading) target model [21, 23]. Collect the target reflectivities with respect to all Txs observed at the n_r th radar Rx in a vector $\mathbf{h}_{n_r} \triangleq [h_{1n_r}, \dots, h_{M_r n_r}]^\top \in \mathbb{C}^{M_r}$.

The velocity of the target is the vector $\boldsymbol{\nu}_t \triangleq (\nu_{x,t}, \nu_{y,t})$, where $\nu_{x,t}$ and $\nu_{y,t}$ are deterministic but unknown horizontal and vertical velocity components in the 2-D plane. The Doppler frequency with respect to the m_r^{th} Tx - n_r^{th} Rx pair is $f_{m_r t n_r} = \frac{\nu_{x,t}}{\lambda} (\cos \theta_{m_r t} + \cos \phi_{n_r t}) + \frac{\nu_{y,t}}{\lambda} (\sin \theta_{m_r t} + \sin \phi_{n_r t})$ [25], where λ denotes the carrier wavelength, θ_{m_r} and ϕ_{n_r} are the angles of departure at the m_r^{th} Tx and angles of arrival at the n_r^{th} Rx, respectively. The narrowband assumption of $s_{m_r}(t)$ allows us to approximate the propagation delay arising from the reflection off an arbitrary scatterer of the n_r^{th} extended target to that from the center of gravity of the n_r^{th} extended target, for all $m_r \in \mathbb{Z}_+(M_r)$ and $n_r \in \mathbb{Z}_+(N_r)$ [21]. If center of gravity of the extended target is (x_t, y_t) , then the propagation delay with respect to m_r^{th} Tx - n_r^{th} Rx is $\zeta_{m_r t n_r} = \frac{\sqrt{(x_{m_r} - x_t)^2 + (y_{m_r} - y_t)^2}}{c} + \frac{\sqrt{(x_{n_r} - x_t)^2 + (y_{n_r} - y_t)^2}}{c}$, where $c = 3 \times 10^8$ m/s is the speed of the light. The slow-motion assumption of the target guarantees that $\zeta_{m_r t n_r}$ is constant during each CPI.

The baseband signal at the n_r^{th} Rx due to reflection off the target during the observation time $t \in [0, KT_r]$ is

$$y_{t, n_r}(t) = \sum_{m_r=1}^{M_r} h_{m_r t n_r} s_{m_r}(t - \zeta_{m_r t n_r}) \quad (2)$$

$$\approx \sum_{m_r=1}^{M_r} \sum_{k=1}^K h_{m_r t n_r} a_{m_r, k} \phi_{m_r}(t - (k-1)T_r - \zeta_{m_r t n_r}) e^{j2\pi f_{m_r t n_r} t}, \quad (3)$$

where $f'_{m_r t n_r} \triangleq f_{m_r t n_r} T_r$ is the normalized Doppler frequency and the approximation in (3) follows from the ‘‘slow target’’, i.e. $f'_{m_r t n_r}$ is constant within a pulse [25, 33]. Collect the exponential terms in a vector $\mathbf{q}_{r, n_r}[k] = [e^{j2\pi(k-1)f'_{1t n_r}}, \dots, e^{j2\pi(k-1)f'_{M_r t n_r}}]^\top \in \mathbb{C}^{M_r}$ and $\mathbf{Q}_{r, n_r}[k] = \text{diag}(\mathbf{q}_{r, n_r}[k])$.

The received signal $y_{r, n_r}(t)$ is sampled at the rate $F_c = 1/T_c$ to yield discrete-time samples $y_{r, n_r}[n]$. These are then processed by a matched filter bank composed of M_r filters, where the m_r^{th} filter is matched to the waveform $\phi_{m_r}(t)$ [33]. The output of the matched filter peaks at the time instant that corresponds to the range location of the target; the range resolution is set by the pulse length T_P [34]. Assuming that the range cells are aligned [24] across all N_r Rx, the target is observed at the n^{th} range cell, where $n = \lfloor \zeta_{m_r t n_r} / T_P \rfloor \in \mathbb{Z}_+\{N\}$ ¹. At the matched filter bank output for the n_r^{th} Rx, denote the received signal samples from a target observed at the n^{th} range cell by a vector $\mathbf{y}_{t, n_r, n} \in \mathbb{C}^K$ such that

$$\mathbf{y}_{t, n_r, n}[k] = \mathbf{h}_{r_t, n_r}^\top \mathbf{Q}_{r, n_r}[k] \mathbf{a}[k] \triangleq \mathbf{h}_{r_t, n_r}^\top \mathbf{s}_{r_t, n_r}[k], \quad k = 1, \dots, K. \quad (4)$$

Note that we focus on the matched filter output at the n^{th} range cell, or cell under test (CUT), and therefore drop the cell index n in the sequel. Here, define $\mathbf{S}_{r, n_r} = [\mathbf{Q}_{r, n_r}[1] \mathbf{a}[1], \dots, \mathbf{Q}_{r, n_r}[K] \mathbf{a}[K]]$.

In practice, apart from the target, the radar also receives echoes from undesired targets or clutter such as buildings and forests. The clutter echoes are treated as signal-dependent interference produced by many independent and unambiguous point-like scatterers [28]. Denote the clutter trail at the CUT of n_r^{th} Rx by a $K \times 1$ vector \mathbf{y}_{c, n_r} whose covariance matrix (CM) is $\mathbf{R}_{c, n_r} \in \mathbb{C}^{K \times K}$, with its $(m, \ell)^{\text{th}}$ element being $\mathbf{R}_{c, n_r}(m, \ell) = \sigma_{c, n_r}^2 \rho_c^{|m-\ell|}$, where σ_{c, n_r}^2 is the clutter power observed by n_r^{th} Rx and ρ is a constant [28].

B. IBFD MU-MIMO Communications

Consider a FD BS equipped with M_c transmit and N_c receive antennas. There are a total of I UL (J DL) UEs, which function in HD mode simultaneously uploading (downloading) packets during a predefined *scheduling window*. Every i^{th} UL (j^{th} DL) UE employs N_i^u

¹In general, the statistical MIMO radar receiver employs data association algorithms to ascertain the location and Doppler frequencies of each target using echoes from all Tx-Rx pairs. These algorithms are beyond the scope of this paper; we refer the reader to standard literature, e.g. [35], for details.

(N_j^d) transmit-receive antennas. To achieve the maximum capacity of the UL channels, assume $M_c \geq \sum_{i=1}^I N_i^u$ [20]. To facilitate the co-design, the length of the scheduling window is same as the radar CPI; hence, the CPI should exceed the maximum latency required by the UL or DL transmissions [36]. Further, the length of a UL/DL frame is identical to the PRI and the duration of UL/DL symbols is same as that of the radar pulses. It follows that the number of the frames transmitted in a given window is K and the number of the symbols sent in each frame is N . In this context, the MIMO radar and IBFD MU-MIMO communications systems are fully synchronous [12].

Denote the number of data streams as $D_i^u \leq N_i^u$. During the l^{th} symbol period of the k^{th} frame, the i^{th} UL UE sends a unit-energy symbol vector $\mathbf{d}_{u,i}[k, l] \in \mathbb{C}^{D_i^u}$ to the BS, where $\mathbf{d}_{u,i}[k, l]$ is independent and identically distributed (i.i.d.) for $i \in \mathbb{Z}_+\{I\}$, $k \in \mathbb{Z}_+\{K\}$, and $l \in \mathbb{Z}_+\{N\}$. The precoder of i^{th} UL UE for the k^{th} frame is the matrix $\mathbf{P}_{u,i}[k] \in \mathbb{C}^{N_i^u \times D_i^u}$ so that the discrete-time transmit signal at this UE is $\mathbf{s}_{u,i}[k, l] = \mathbf{P}_{u,i}[k] \mathbf{d}_{u,i}[k, l]$. The UL from the i^{th} UL UE to the BS is a multiple access channel (MAC) $\mathbf{H}_{i,B} \in \mathbb{C}^{M_c \times N_i^u}$. The analog received signal is processed through conventional stages such as downconversion, symbol rate sampling, matched filtering, and time/frequency synchronization. The resulting discrete-time received signal at the BS from the i^{th} UL UE is [37]

$$\mathbf{y}_{i,B}[k, l] = \mathbf{H}_{i,B} \mathbf{s}_{u,i}[k, l]. \quad (5)$$

At the i^{th} UL UE, the simultaneous transmissions of the rest of UL UEs lead to the multi-user interference (MUI)²

$$\mathbf{y}_{\text{um},i}[k, l] = \sum_{q \neq i} \mathbf{H}_{q,B} \mathbf{s}_{u,q}[k, l]. \quad (6)$$

The CMs of $\mathbf{y}_{i,B}[k, l]$ and $\mathbf{y}_{\text{um},i}[k, l]$ are $\mathbf{R}_{u,i}[k, l] = \mathbf{H}_{i,B} \mathbf{P}_{u,i}[k] \mathbf{P}_{u,i}^\dagger[k] \mathbf{H}_{i,B}^\dagger$ and $\mathbf{R}_{\text{um},i}[k, l] = \sum_{g \neq i} \mathbf{H}_{g,B} \mathbf{P}_{u,g} \mathbf{P}_{u,g}^\dagger \mathbf{H}_{g,B}^\dagger$, respectively.

At the DL, the J UEs simultaneously download packets from the BS. During the l^{th} symbol period of the k^{th} frame, the symbol vector intended for the j^{th} DL UE is $\mathbf{d}_{d,j}[k, l] \in \mathbb{C}^{D_j^d}$, i.i.d in k and l , where $D_j^d \leq \min(M_c, N_j^d)$ denotes the number of unit-energy data streams. Given the precoding matrix for the j^{th} DL UE at the k^{th} frame as $\mathbf{P}_{d,j}[k] \in \mathbb{C}^{M_c \times D_j^d}$, the signal vector transmitted from the BS to the j^{th} DL UE is $\mathbf{s}_{d,j}[k, l] = \mathbf{P}_{d,j}[k] \mathbf{d}_{d,j}[k, l]$. The channel between the BS and the j^{th} DL UE is a broadcast (BC) channel $\mathbf{H}_{B,j} \in \mathbb{C}^{N_j^d \times M_c}$. The $\mathbf{H}_{B,j}$ is full rank for all j to achieve the highest spatial degrees of freedom of the MIMO-BC channel [20]. After similar conventional processing as in the BS above, the resulting discrete-time DL signal at the j^{th} DL UE is [37]

$$\mathbf{y}_{B,j}[k, l] = \mathbf{H}_{B,j} \mathbf{s}_{d,j}[k, l] + \mathbf{y}_{\text{dm},j}[k, l], \quad (7)$$

where $\mathbf{y}_{\text{dm},j}[k, l] = \mathbf{H}_{B,j} \sum_{g \neq j} \mathbf{s}_{d,g}[k, l]$ denotes the MUI of the j^{th} DL UE. Using the fact that the symbol vectors are i.i.d., the CMs of $\mathbf{y}_{B,j}[k, l]$ and $\mathbf{y}_{\text{dm},j}[k, l]$ are $\mathbf{R}_{\text{dm},j}[k, l] = \sum_{g \neq j} \mathbf{H}_{B,j} \mathbf{P}_{d,g}[k] \mathbf{P}_{d,g}^\dagger[k] \mathbf{H}_{B,j}^\dagger$ and $\mathbf{R}_{B,j}[k, l] = \mathbf{R}_{\text{dm},j}[k, l] + \mathbf{H}_{B,j} \mathbf{P}_{d,j}[k] \mathbf{P}_{d,j}^\dagger[k] \mathbf{H}_{B,j}^\dagger$, respectively.

The FD transmission of the BS implies that its Rx is overlaid with the DL signals which are transmitted over the self-interference channel $\mathbf{H}_{\text{BB}} \in \mathbb{C}^{N_c \times M_c}$. The self-interfering signal at the BS Rx is

$$\mathbf{y}_{\text{BB}}[k, l] = \mathbf{H}_{\text{BB}} \sum_{j=1}^J \mathbf{P}_{d,j}[k] \mathbf{d}_{B,j}[k, l]. \quad (8)$$

In the simultaneous UL-DL transmissions, the channel from i^{th} UL UE to j^{th} DL UE is $\mathbf{H}_{i,j} \in \mathbb{C}^{N_j^d \times N_i^u}$, with the CM $\mathbf{R}_{\text{BB}}[k, l] = \sum_{j=1}^J \mathbf{H}_{B,j} \mathbf{P}_{d,j}[k] \mathbf{P}_{d,j}^\dagger[k] \mathbf{H}_{\text{BB}}^\dagger$. Hence, the UL signal received at the j^{th} DL UE during the l^{th} symbol period of the k^{th} frame is

²The MU transmission here is via linear precoders which have lower complexity than the optimal dirty paper coding [20].

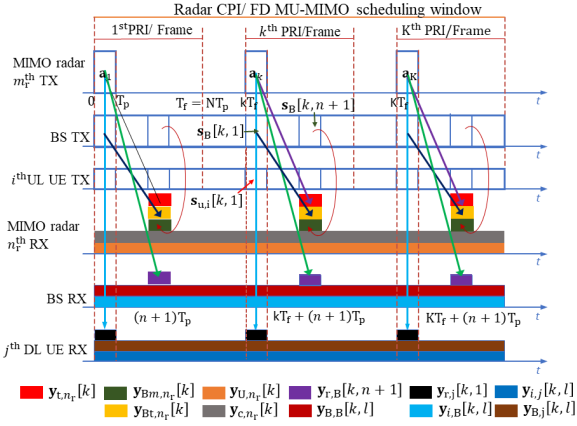


Fig. 2. The overlaid signal timing diagram for one CPI is illustrated where the unit time scale is the pulse or symbol duration. For each MIMO radar Rx, we focus on the n^{th} range cell where the target is observed. The j^{th} UE is interfered by the radar probing signal during the symbol period when the MIMO radar transmits pulses.

$$\mathbf{y}_{u,j}[k, l] = \sum_{i=1}^I \mathbf{H}_{i,j} \mathbf{P}_{u,i}[k] \mathbf{d}_{u,i}[k, l], \quad (9)$$

with the CM $\mathbf{R}_{u,j}[k, l] = \sum_{i=1}^I \mathbf{H}_{i,j} \mathbf{P}_{u,i}[k] \mathbf{P}_{u,i}^\dagger[k] \mathbf{H}_{i,j}^\dagger$. Assume perfect CSI at the Tx and Rx (CSITR) is available to the IBFD MU-MIMO communications as well as radar. The elements of $\mathbf{H}_{B,j}$, $\mathbf{H}_{i,B}$, $\mathbf{H}_{i,j}$, and $\mathbf{H}_{B,B}$ are distributed as $\mathcal{CN}(0, \eta_{d,j}^2)$, $\mathcal{CN}(0, \eta_{u,i}^2)$, $\mathcal{CN}(0, \eta_{i,j}^2)$, and $\mathcal{CN}(0, \eta_{BB}^2)$, respectively, for all i and j .

C. Joint Radar-Communications

In joint radar-communications, the radar Rx signal is overlaid with the IBFD MU-MIMO communications signals leading to additional challenges in target detection. Similarly, the radar probing signals adversely impact the UL/DL rates. We now define the overlaid signals at the MIMO radar Rx (with contributions from the target, clutter, UL, direct DL, indirect DL, and noise) and BS (see Fig. 2).

The DL signal $\mathbf{s}_{d,j}[k, l]$ is received at the n_r^{th} radar Rx through a multi-path fading channel $\mathbf{h}_{Bm,n_r} \in \mathbb{C}^{M_c} \sim \mathcal{CN}(0, \eta_{Bm,n_r}^2 \mathbf{I}_{M_c})$ over a CPI. Assume that the time delay between the BS and each radar Rx is negligible. The DL signal at n_r^{th} radar Rx in k^{th} PRI is

$$\mathbf{y}_{Bm,n_r}[k] = \mathbf{h}_{Bm,n_r}^\top e^{j2\pi(k-1)f_{Bm,n_r}} \sum_{j=1}^J \mathbf{s}_{d,j}[k, n+1], \quad (10)$$

where f_{Bm,n_r} denotes the normalized channel Doppler frequency.

When a target is present, the n_r^{th} radar Rx also receives the echoes of the DL signals reflected off the target through a reflection channel $\mathbf{h}_{Bt,n_r} \sim \mathcal{CN}(0, \eta_{Bt,n_r}^2 \mathbf{I})$. Throughout this paper, we assume that $\eta_{n_r}^2$ and η_{Bt,n_r}^2 are perfectly known to the BS, all UEs and MIMO radar Rxs. Without loss of generality, consider a fully synchronous scenario, wherein $\mathbf{s}_{d,j}[k]$ is reflected off the target before received by the n_r^{th} radar Rx in each PRI over the channel \mathbf{h}_{Bt,n_r} . Denote the target's normalized Doppler frequency by f_{Bt,n_r} . The target echo from reflected DL signal at CUT of n_r^{th} radar Rx during k^{th} PRI is

$$\mathbf{y}_{Bt,n_r}[k] = \mathbf{h}_{Bt,n_r}^\top e^{j2\pi(k-1)f_{Bt,n_r}} \sum_{j=1}^J \mathbf{s}_{d,j}[k, 1]. \quad (11)$$

Note that the target information is embedded in only \mathbf{y}_{Bt,n_r} . Hence, the effective number of antennas to detect the target is $M = M_c + M_r$. The overall radar target channel matrix is $\mathbf{h}_{t,n_r} = [\mathbf{h}_{rt,n_r}^\top, \mathbf{h}_{Bt,n_r}^\top]^\top \in \mathbb{C}^M$ whose CM is $\mathbb{E}[\mathbf{h}_{t,n_r} \mathbf{h}_{t,n_r}^\dagger] \triangleq \mathbf{\Sigma}_{t,n_r} = \eta_{rt,n_r}^2 \mathbf{I} \oplus \eta_{Bt,n_r}^2 \mathbf{I}$. Denote $\mathbf{s}_{rt,n_r}[k] = \mathbf{Q}_{r,n_r}[k] \mathbf{a}[k]$ and $\mathbf{s}_{Bt,n_r}[k] = e^{j2\pi(k-1)f_{Bt,n_r}} \sum_{j=1}^J \mathbf{s}_{d,j}[k]$, and define $\mathbf{s}_{t,n_r}[k] = [\mathbf{s}_{rt,n_r}[k], \mathbf{s}_{Bt,n_r}[k]]^\top = \mathbf{J}_r \mathbf{s}_{rt,n_r}[k] + \mathbf{J}_B \mathbf{s}_{Bt,n_r}[k]$, where $\mathbf{J}_r = [\mathbf{I}_{M_r \times M_r}; \mathbf{0}_{M_c \times M_r}] \in \mathbb{R}^{M \times M_r}$ and $\mathbf{J}_B = [\mathbf{0}_{M_r \times M_c}; \mathbf{I}_{M_c \times M_c}] \in$

$\mathbb{R}^{M \times M_c}$. Combining the echoes from the DL link and the radar Tx, the target signal becomes

$$\mathbf{y}_{t,n_r}[k] \triangleq \mathbf{h}_{rt,n_r}^\top \mathbf{s}_{rt,n_r}[k] + \mathbf{h}_{Bt,n_r}^\top \mathbf{s}_{Bt,n_r}[k]. \quad (12)$$

For a given CPI, denote $\mathbf{y}_{Bm,n_r} \triangleq [y_{Bm,n_r}(1), \dots, y_{Bm,n_r}(K)]^\top$ and $\mathbf{y}_{Bt,n_r} \triangleq [y_{Bt,n_r}(1), \dots, y_{Bt,n_r}(K)]^\top$. The CMs of \mathbf{y}_{Bm,n_r} and \mathbf{y}_{t,n_r} are, respectively, \mathbf{R}_{Bm,n_r} and \mathbf{R}_{t,n_r} such that

$$\begin{aligned} \mathbf{R}_{Bm,n_r}(m, \ell) &\triangleq \mathbb{E}[y_{Bm,n_r}[m] y_{Bm,n_r}^*[m]] \\ &= \eta_{Bm,n_r}^2 e^{j2\pi(m-\ell)f_{Bm,n_r}} \sum_{j=1}^J \mathbf{s}_{d,j}^\dagger(\ell, n+1) \sum_{j=1}^J \mathbf{s}_{d,j}(m, n+1), \end{aligned}$$

and

$$\begin{aligned} \mathbf{R}_{t,n_r}(m, \ell) &\triangleq \mathbb{E}[y_{t,n_r}[m] y_{t,n_r}^*[m]] \\ &= \eta_{rt,n_r}^2 \mathbf{s}_{rt,n_r}^\dagger[\ell] \mathbf{s}_{rt,n_r}[m] + \eta_{Bt,n_r}^2 \mathbf{s}_{Bt,n_r}^\dagger[\ell] \mathbf{s}_{Bt,n_r}[m]. \end{aligned}$$

Similarly, the UL signals are also intercepted by the n_r^{th} radar Rx throughout the CPI and the ones observed at the CUT of the n_r^{th} radar Rx are $(n+1)^{\text{th}}$ symbols, i.e. $\mathbf{s}_{u,i}[k]$ for all i and k . However, unlike the DL model, the transmit power of UL UEs is relatively low. Therefore, it is possible to ignore the reflections of UL signals off the targets. The channel from i^{th} UL UE to n_r^{th} MIMO radar Rx is $\mathbf{h}_{i,n_r} \sim \mathcal{CN}(0, \eta_{i,n_r}^2 \mathbf{I}_{N_r^u})$, i.i.d in i and n_r . The UL signal at the CUT of the n_r^{th} radar Rx during the k^{th} PRI is

$$\mathbf{y}_{U,n_r}[k] = \sum_{i=1}^I \mathbf{h}_{i,n_r}^\top e^{j2\pi(k-1)f_{i,n_r}} \mathbf{s}_{u,i}[k], \quad (13)$$

where f_{i,n_r} denotes the normalized channel Doppler shift. Combining the UL signals for all K PRIs yields the total UL received sample vector for the n_r^{th} radar Rx as $\mathbf{y}_{U,n_r} = [y_{U,n_r}(1), \dots, y_{U,n_r}(K)]^\top$, with the CM \mathbf{R}_{U,n_r} , whose $(m, \ell)^{\text{th}}$ element is

$$\begin{aligned} \mathbf{R}_{U,n_r}(m, \ell) &\triangleq \mathbb{E}[y_{U,n_r}[m] y_{U,n_r}^*[m]] \\ &= \sum_{i=1}^I \eta_{i,n_r}^2 e^{j2\pi(m-\ell)f_{i,n_r}} \mathbf{s}_{i,n_r}^\dagger[\ell, n+1] \mathbf{s}_{i,n_r}[m, n+1]. \end{aligned}$$

Denote the CSCG noise vector at the n_r^{th} radar Rx by $\mathbf{z}_{r,n_r} \in \mathcal{CN}(\mathbf{0}, \sigma_{r,n_r}^2 \mathbf{I})$. Combining this noise with (10), (12), clutter trail, and (13), the receive signal at the CUT of the n_r^{th} radar Rx is

$$\mathbf{y}_{r,n_r} = \mathbf{y}_{t,n_r} + \underbrace{\mathbf{y}_{c,n_r} + \mathbf{y}_{Bm,n_r} + \mathbf{y}_{U,n_r}}_{\mathbf{y}_{in,n_r}} + \mathbf{z}_{r,n_r}, \quad (14)$$

where \mathbf{y}_{in,n_r}^\top represents the interference-plus-noise (IN) component of \mathbf{y}_{r,n_r} . The CMs of \mathbf{y}_{in,n_r} and \mathbf{y}_{r,n_r} are $\mathbf{R}_{in,n_r}^\dagger \triangleq \mathbf{R}_{c,n_r} + \mathbf{R}_{Bm,n_r} + \mathbf{R}_{U,n_r} + \sigma_{r,n_r}^2 \mathbf{I}$ and $\mathbf{R}_{r,n_r} = \mathbf{R}_{t,n_r} + \mathbf{R}_{in,n_r}^\dagger$, respectively.

Over the course of the CPI, the radar probing pulses interfere with the BS and DL UEs intermittently. As shown in Fig. 2, the j^{th} DL UE receives the radar signals radiated by the m_r^{th} radar Tx through a fading channel $\mathbf{h}_{m_r,j}$ within the 1st symbol period of each frame. Because of relatively small effective antenna apertures of the DL UEs, the radar signal reflected by the target toward the DL UEs is ignored. Denote the channel matrix from the M_r MIMO radar Tx to the j^{th} DL UE by $\mathbf{H}_{r,j} \triangleq [\mathbf{h}_{1,j}, \dots, \mathbf{h}_{M_r,j}]$, where $\mathbf{h}_{m_r,j} \sim \mathcal{CN}\left(\sqrt{\frac{\kappa}{\kappa+1}} \boldsymbol{\mu}_{m_r,j}, \frac{\eta_{m_r,j}^2}{\kappa+1} \mathbf{I}_{N_j^d}\right)$, where κ denotes the K -factor, and $\boldsymbol{\mu}_{m_r,j}$ the specular path gains, and $\eta_{m_r,j}^2$ the variances of the scattered path for all m_r and j . The radar signal intercepted by the j^{th} DL UE at the l^{th} symbol period of the k^{th} frame is

$$\mathbf{y}_{r,j}[k, l] = \begin{cases} \mathbf{H}_{r,j} \mathbf{a}_k, & l = 1, \\ \mathbf{0}, & l \neq 1, \end{cases} \quad (15)$$

where $\mathbf{H}_{r,j}$ along with its channel Doppler is usually estimated by transmitting known training symbols [12]. Then, the CM of $\mathbf{y}_{r,j}[k, l]$ is $\mathbf{R}_{r,j}[k, 1] = \mathbf{H}_{r,j} \mathbf{a}_k \mathbf{a}_k^\dagger \mathbf{H}_{r,j}^\dagger$. Combining (7), (9), and (15) with noise, the received signal at the j^{th} DL UE is

$$\mathbf{y}_{d,j}[k, l] = \mathbf{y}_{B,j}[k, l] + \mathbf{y}_{u,j}[k, l] + \mathbf{y}_{r,j}[k, l] + \mathbf{z}_{d,j}[k, l], \quad (16)$$

where $\mathbf{z}_{d,j}[k, l]$ is the CSCG noise vector at the j^{th} DL UE, i.i.d in k and l . The CM of $\mathbf{y}_{d,j}[k, l]$ is $\mathbf{R}_j^d[k, l] = \mathbf{R}_{B,j}[k, l] + \mathbf{R}_{in,j}^d[k, l]$, where $\mathbf{R}_{in,j}^d[k, l] = \mathbf{R}_{dm,j}[k, l] + \mathbf{R}_{U,j}[k, l] + \mathbf{R}_{r,j}[k, l] + \sigma_j^2 \mathbf{I}_{N_j^d}$ denotes the IN CM of $\mathbf{y}_j[k, l]$.

Unlike the DL UEs, the BS is equipped with an antenna array with a higher gain and larger aperture. Therefore, it captures the radar signals reflected off the target and clutter. The radar signals reflected off the target and clutter toward the BS Rx during the $(n+1)^{\text{th}}$ symbol period of each frame interfere with the BS throughout the CPI (see Fig. 2). Denote the channel matrix between the M_r MIMO radar TxS and the BS Rx as $\mathbf{H}_{rB} = [\mathbf{h}_{1,B}, \dots, \mathbf{h}_{M_r,B}] \in \mathbb{C}^{M \times M_r}$, where $\mathbf{h}_{m_r,B} \sim \mathcal{CN}\left(\sqrt{\frac{\kappa}{\kappa+1}} \boldsymbol{\mu}_{m_r,B}, \frac{\eta_{m_r,B}}{\kappa+1} \mathbf{I}_{N_j^d}\right)$. The radar signals observed at the BS for the l^{th} symbol period of the k^{th} frame is

$$\mathbf{y}_{rB}[k, l] = \begin{cases} \mathbf{H}_{rB} \mathbf{a}_k, & l = n+1, \\ \mathbf{0}, & l \neq n+1, \end{cases} \quad (17)$$

whose CM is $\mathbf{R}_{rB}[k] = \mathbf{H}_{rB} \mathbf{a}_k \mathbf{a}_k^\dagger \mathbf{H}_{rB}^\dagger$. The CSCG noise vector measured at the BS Rx is $\mathbf{z}_B[k, l] \sim \mathcal{CN}(0, \sigma_B^2 \mathbf{I}_{M_C})$. Then, combining this noise trail with (5), (6), (8), and (17), the received signal at the BS Rx required to decode $\mathbf{s}_{u,i}[k, l]$ is

$$\mathbf{y}_{u,i}[k, l] = \mathbf{y}_{i,B}[k, l] + \mathbf{y}_{um,i}[k, l] + \mathbf{y}_{BB}[k, l] + \mathbf{y}_{rB}[k, l] + \mathbf{z}_B[k, l].$$

The CMs of IN at the i^{th} UL UE is $\mathbf{R}_{in,i}^u[k, l] = \mathbf{R}_{um,i}^u[k, l] + \mathbf{R}_{BB}[k, l] + \mathbf{R}_{rB}[k, l] + \sigma_B^2 \mathbf{I}_{M_C}$ and that of $\mathbf{y}_{u,i}[k, l]$ as $\mathbf{R}_i^u[k, l] = \mathbf{R}_{i,B}[k, l] + \mathbf{R}_{in,i}^u[k, l]$.

The $\mathbf{y}_{rB}[k, l]$ and $\mathbf{y}_{r,j}[k, l]$ are non-zero only when $l = n+1$ and $l = 1$, respectively. Therefore, we focus on the performances of DL and UL at the $(n+1)^{\text{th}}$ and 1^{st} symbol periods of each frame, respectively. In the sequel, for notational simplicity, we omit the symbol period index l .

III. CWSM MAXIMIZATION

The performance metrics to design radar and communications systems are not identical because of different system goals. For example, in general, a communications system strives to achieve high data rates while a radar performs detection, estimation, and tracking. Some recent works [17, 19] suggest MI as a common performance metric. The MI is a well-studied metric in MU-MIMO communications for transmit precoder design [38]. The seminal work on radar waveform design metric by [39] originally proposed MI as a measure of radar performance. Later, MI-based waveform design was also extended to MIMO radars [27, 28]. It has been shown [27] that maximizing the MI between the radar received signal and the target response leads to a better detection performance in the presence of the Gaussian noise. For our co-design, we propose a more effective common performance measure by combining the MI-based information theoretic perspective of radar waveform design with the conventional weighted sum rate maximization for MU-MIMO systems into a new CWSM metric.

To derive CWSM, denote the LRF at the n_r^{th} MIMO radar Rx by $\mathbf{U}_{r,n_r} = [\mathbf{u}_{r,n_r}(1), \dots, \mathbf{u}_{r,n_r}(K)] \in \mathbb{C}^{M \times K}$. Define $\mathbf{S}_{t,n_r} = [\mathbf{s}_{t,n_r}(1), \dots, \mathbf{s}_{t,n_r}(K)]$. Passing (14) through the LRF \mathbf{U}_{r,n_r} gives

$$\begin{aligned} \tilde{\mathbf{y}}_{r,n_r} &= \underbrace{\mathbf{U}_{r,n_r} \mathbf{S}_{t,n_r} \mathbf{h}_{t,n_r}}_{\tilde{\mathbf{y}}_{t,n_r}} + \underbrace{\mathbf{U}_{r,n_r} \mathbf{y}_{in,n_r}}_{\tilde{\mathbf{y}}_{in,n_r}} \\ &= \sum_{k=1}^K \mathbf{u}_{r,n_r}[k] \{ \mathbf{y}_{t,n_r}[k] + \mathbf{y}_{in,n_r}[k] \}. \end{aligned} \quad (18)$$

Since \mathbf{h}_{t,n_r} holds the target information, the MI between $\tilde{\mathbf{y}}_{r,n_r}$ and \mathbf{h}_{t,n_r} conditioned on the radar code matrix \mathbf{A} is derived using chain rule as [40]

$$\begin{aligned} I_{r,n_r} &\triangleq I(\tilde{\mathbf{y}}_{r,n_r}; \mathbf{h}_{t,n_r} | \mathbf{A}) = H(\tilde{\mathbf{y}}_{r,n_r} | \mathbf{A}) - H(\tilde{\mathbf{y}}_{r,n_r} | \mathbf{h}_{t,n_r}, \mathbf{A}) \\ &= H(\tilde{\mathbf{y}}_{r,n_r} | \mathbf{A}) - H(\tilde{\mathbf{y}}_{t,n_r} | \mathbf{h}_{t,n_r}, \mathbf{A}) - H(\tilde{\mathbf{y}}_{in,n_r} | \mathbf{h}_{t,n_r}, \mathbf{A}) \\ &= H(\tilde{\mathbf{y}}_{r,n_r} | \mathbf{A}) - H(\tilde{\mathbf{y}}_{in,n_r} | \mathbf{A}), \end{aligned} \quad (19)$$

where the last equality holds because $\tilde{\mathbf{y}}_{in,n_r}$ completely depends on \mathbf{A} such that $H(\tilde{\mathbf{y}}_{t,n_r} | \mathbf{h}_{t,n_r})$ and \mathbf{h}_{t,n_r} as well as $\tilde{\mathbf{y}}_{in,n_r}$ and \mathbf{h}_{t,n_r} are mutually independent. By the definition of the conditional differential entropy with the Gaussian noise [40], we get

$$\begin{aligned} H(\tilde{\mathbf{y}}_{r,n_r} | \mathbf{A}) &= \varrho + \log |\mathbf{U}_{r,n_r} \mathbf{R}_{r,n_r} \mathbf{U}_{r,n_r}^\dagger|, \\ H(\tilde{\mathbf{y}}_{in,n_r} | \mathbf{A}) &= \varrho + \log |\mathbf{U}_{r,n_r} \mathbf{R}_{in,n_r} \mathbf{U}_{r,n_r}^\dagger|, \end{aligned}$$

where the constant $\varrho = K \log(\pi) + K$. This leads to

$$\begin{aligned} I_{r,n_r} &= \log \frac{|\mathbf{U}_{r,n_r} (\mathbf{R}_{t,n_r} + \mathbf{R}_{in,n_r}) \mathbf{U}_{r,n_r}^\dagger|}{|\mathbf{U}_{r,n_r} \mathbf{R}_{in,n_r} \mathbf{U}_{r,n_r}^\dagger|} \\ &= \log \left| \mathbf{I} + \mathbf{U}_{r,n_r} \mathbf{R}_{t,n_r} \mathbf{U}_{r,n_r}^\dagger (\mathbf{U}_{r,n_r} \mathbf{R}_{in,n_r} \mathbf{U}_{r,n_r}^\dagger)^{-1} \right|. \end{aligned} \quad (20)$$

The LRFs deployed at the BS for the i^{th} UL UE and the j^{th} DL UE during the k^{th} frame are $\mathbf{U}_{u,i}[k] \in \mathbb{C}^{d_i^u \times N_C}$ and $\mathbf{U}_{d,j}[k] \in \mathbb{C}^{d_j^d \times N_i^d}$, respectively. Denote the outputs of $\mathbf{U}_{u,i}[k]$ and $\mathbf{U}_{d,j}[k]$ by $\tilde{\mathbf{y}}_{u,i}[k]$ and $\tilde{\mathbf{y}}_{d,j}[k]$, respectively. The MI between $\tilde{\mathbf{y}}_{u,i}[k]$ and $\mathbf{s}_{i,B}[k]$ is

$$\begin{aligned} I_{u,i}[k] &\triangleq I(\mathbf{s}_{i,B}[k]; \tilde{\mathbf{y}}_i[k, l] | \mathbf{H}_{i,B}) = \\ &\log \left| \mathbf{I} + \mathbf{U}_{u,i}[k] \mathbf{R}_{u,i}^u[k] \mathbf{U}_{u,i}^\dagger[k] \left(\mathbf{U}_{u,i}[k] \mathbf{R}_{in,i}^u[k] \mathbf{U}_{u,i}^\dagger[k] \right)^{-1} \right|, \end{aligned} \quad (21)$$

and that between $\tilde{\mathbf{y}}_{d,j}[k]$ and $\mathbf{s}_{B,j}[k]$ is

$$\begin{aligned} I_{d,j}[k, l] &\triangleq I(\mathbf{s}_{B,j}[k]; \tilde{\mathbf{y}}_j[k, l] | \mathbf{H}_{B,j}) = \\ &\log \left| \mathbf{I} + \mathbf{U}_{d,j}[k] \mathbf{R}_j^d[k] \mathbf{U}_{d,j}^\dagger[k] \left(\mathbf{U}_{d,j}[k] \mathbf{R}_{in,j}^d[k] \mathbf{U}_{d,j}^\dagger[k] \right)^{-1} \right|. \end{aligned} \quad (22)$$

The weighted sum of the MIs at all radar RxS, BS, and DL UEs for the entire CPI is the CWSM

$$I_{CWSM} = \sum_{n_r=1}^{N_r} \alpha_{n_r}^r I_{r,n_r} + \sum_{k=1}^K \sum_{i=1}^I \alpha_i^u I_i^u[k] + \sum_{k=1}^K \sum_{j=1}^J \alpha_j^d I_j^d[k], \quad (23)$$

where $\alpha_{n_r}^r$, α_i^u , and α_j^d are pre-defined priority weights given to the n_r^{th} MIMO radar Rx, i^{th} UL UE and j^{th} DL UE, respectively, for all n_r , i , and j [31, 41, 42].

Define the set of all UL and DL precoders as $\{\mathbf{P}\} \triangleq \{\mathbf{P}_{u,i}[k], \mathbf{P}_{d,j}[k] | i \in \mathbb{Z}_+\{I\}, j \in \mathbb{Z}_+\{J\}, k \in \mathbb{Z}_+\{K\}\}$ and the set of all LRFs at BS Rx, DL UEs, and radar RxS as $\{\mathbf{U}\} \triangleq \{\mathbf{U}_{u,i}[k], \mathbf{U}_{d,j}[k], \mathbf{U}_{r,n_r} | i \in \mathbb{Z}_+\{I\}, j \in \mathbb{Z}_+\{J\}, k \in \mathbb{Z}_+\{K\}, n_r \in \mathbb{Z}_+\{N_r\}\}$. Assume that the DL and UL link budgets mandate maximum power as P_B and P_U , respectively. The j^{th} DL and i^{th} UL transmit powers at the k^{th} frame are $P_{d,j} = \text{Tr}\{\mathbf{P}_{d,j}[k] \mathbf{P}_{d,j}^\dagger[k]\}$

and $P_{u,i} = \text{Tr}\{\mathbf{P}_{u,i}[k] \mathbf{P}_{u,i}^\dagger[k]\}$, respectively; these must be smaller than the link budget powers. Denote the least acceptable achievable rates for the UL and DL by R_{UL} and R_{DL} , respectively; these determine the QoS of the IBFD MU-MIMO.

Then, we jointly design the UL/DL precoding matrices $\{\mathbf{P}\}$, radar code matrix \mathbf{A} , and LRFs $\{\mathbf{U}\}$ by maximizing CWSM in the following optimization problem

$$\begin{aligned} &\underset{\{\mathbf{P}\}, \{\mathbf{U}\}, \mathbf{A}}{\text{maximize}} && I_{CWSM}(\{\mathbf{U}\}, \{\mathbf{P}\}, \mathbf{A}) \end{aligned} \quad (24a)$$

$$\text{subject to} \quad \sum_{j=1}^J P_{B,j}[k] \leq P_B, \quad (24b)$$

$$P_{u,i} \leq P_U, \quad (24c)$$

$$R_{u,i}[k] \geq R_{UL}, \quad (24d)$$

$$R_{d,j}[k] \geq R_{DL}, \quad (24e)$$

$$\|\mathbf{a}_{m_r}\|^2 = P_{r,m_r}, \quad (24f)$$

$$\frac{K \max_{k=1, \dots, K} \|\mathbf{a}_{m_r}[k]\|^2}{P_{r,m_r}} \leq \gamma_{m_r}, \quad \forall i, j, k, m_r, \quad (24g)$$

where the constraints (24f) and (24g) are determined by the transmit power and PAR of the m_r^{th} MIMO radar Tx, respectively. Note that the PAR constraint is applied column-wise to the code matrix \mathbf{A} because antennas of statistical MIMO radar are widely distributed.

IV. JOINT WAVEFORM-PRECODER-FILTER DESIGN

Even without non-convex constraints (24d)-(24g), the optimization in (24) is non-convex because the objective function I_{CWSM} is not jointly concave over $\{\mathbf{P}\}$, $\{\mathbf{U}\}$, and \mathbf{A} , and therefore its global optima are generally intractable [42]. In general, such a problem is solved by alternately optimizing over one unknown variable at a time. When the number of variables is large, methods such as BCD partition the all optimization variables into, say, V small groups or blocks and optimize over each block, one at a time, while keeping other block variables fixed [43]. The net effect is that the problem is equivalently solved by iteratively solving less complex V subproblems. If there are only two blocks of variables, BCD reduces to the classical alternating minimization method [43, 44].

It has been shown [45, 46] that BCD converges globally to a stationary point for both convex and non-convex problems while methods such as Alternating Direction Method of Multipliers (ADMM) and Douglas-Rachford Splitting (DRS) achieve only linear convergence for strictly convex and some non-convex (e.g. multi-convex) problems. The stochastic gradient descent (SGD) used to address saddle point problems has a slower convergence rate than BCD and offers only weak convergence for non-convex problems [46].

A natural way to group the block coordinate variables to solve (24) is to make blocks of $\{\mathbf{P}\}$, \mathbf{A} , and $\{\mathbf{U}\}$. At each iteration, we apply *direct update* [43], i.e. maximize I_{CWSM} for all the block variables. Further, we update the block variables in a cyclic sequence because its global and local convergence has been well-established [15, 43] compared to other sequential update rules³. In particular, we adopt the Gauss-Seidel BCD [43], which minimizes the objective function cyclically over each block while keeping the other blocks fixed.

A summary of our strategy is as follows. Note that $\{\mathbf{P}\}$ is subject to only communications-centric constraints (24b)-(24e) and \mathbf{A} to both radar-centric PAR and communications-centric constraints (24f)-(24g). We denote the sets of feasible \mathbf{A} determined by the communications-centric and PAR constraints by \mathbb{A}_c and \mathbb{A}_r , respectively. Therefore, the optimal solution \mathbf{A}^* is a point in the intersection of \mathbb{A}_c and \mathbb{A}_r , namely, $\mathbf{A}^* \subseteq \mathbb{A}_c \cap \mathbb{A}_r$. The AP method [47, 48] is appropriate to perform this search for \mathbf{A}^* . We first transform the I_{CWSM} maximization problem in (24) to a weighted minimum mean-squared-error (WMMSE) minimization problem without the PAR constraints in Section IV-A. The concept of maximizing information theoretic quantities via WMMSE has been explored for precoder design in MIMO communications [31, 38] with better results than techniques like geometric programming. These low complexity methods guarantee convergence to at least a local optimum [38]. In Section IV-B, we then employ BCD in our proposed WMMSE-MRMC algorithm to solve for the optimal \mathbf{A} in \mathbb{A}_c , which we denote as \mathbf{A}' , and the optimal $\{\mathbf{P}^*\}$. Then, using AP, we project each column of \mathbf{A}' onto \mathbb{A}_r in Section IV-C. The WMMSE-MRMC and AP procedures comprise the overall BCD-AP MRMC algorithm (Section IV-D) and are repeated recursively till convergence.

A. Relationship between WMMSE and MI

Recall CWSM maximization in (24) without PAR constraints, i.e.,

$$\underset{\{\mathbf{P}\}, \{\mathbf{U}\}, \mathbf{A}}{\text{maximize}} \quad I_{\text{CWSM}}(\{\mathbf{U}\}, \{\mathbf{P}\}, \mathbf{A}) \quad \text{subject to (24b) - (24d)}. \quad (25)$$

To estimate error in radar processing, the output of LRF at each receiver is compared with the corresponding radar target channel. For error in communications, the LRF output should be compared with the symbol vector. Hence, define the mean squared error (MSE) for the n_r^{th} radar Rx, i^{th} UL UE, and j^{th} DL UE as

³Recently, randomized BCD has also gained more attention when the sequences or iterates generated by BCD are divergent; otherwise, cyclic BCD may still outperform the randomized BCD [45].

$$\begin{aligned} \mathbf{E}_{r,n_r} &= \mathbb{E} \left[(\mathbf{h}_{t,n_r} - \mathbf{U}_{r,n_r} \mathbf{y}_{n_r}^r) (\mathbf{h}_{t,n_r} - \mathbf{U}_{r,n_r} \mathbf{y}_{n_r}^r)^\dagger \right] \\ &= \boldsymbol{\Sigma}_{t,n_r} - 2\mathbf{U}_{r,n_r} \mathbf{S}_{t,n_r} \boldsymbol{\Sigma}_{t,n_r} + \mathbf{U}_{r,n_r} \mathbf{R}_{r,n_r} \mathbf{U}_{r,n_r}^\dagger, \end{aligned} \quad (26)$$

$$\begin{aligned} \mathbf{E}_{u,i}[k] &= \mathbb{E} \left[(\mathbf{d}_{u,i}[k] - \mathbf{U}_{u,i}[k] \mathbf{y}_{u,i}[k]) (\mathbf{d}_{u,i}[k] - \mathbf{U}_{u,i}[k] \mathbf{y}_{u,i}[k])^\dagger \right] \\ &= \mathbf{I} - 2\mathbf{U}_{u,i}[k] \mathbf{H}_{i,B} \mathbf{P}_{u,i}[k] + \mathbf{U}_{u,i}[k] \mathbf{R}_{i,B}^u[k] \mathbf{U}_{u,i}^\dagger[k], \end{aligned} \quad (27)$$

$$\begin{aligned} \mathbf{E}_{d,j}[k] &= \mathbb{E} \left[(\mathbf{d}_{d,j}[k] - \mathbf{U}_{d,j}[k] \mathbf{y}_{d,j}[k]) (\mathbf{d}_{d,j}[k] - \mathbf{U}_{d,j}[k] \mathbf{y}_{d,j}[k])^\dagger \right] \\ &= \mathbf{I} - 2\mathbf{U}_{d,j}[k] \mathbf{H}_{B,j} \mathbf{P}_{d,j}[k] + \mathbf{U}_{d,j}[k] \mathbf{R}_{j,B}^d[k] \mathbf{U}_{d,j}^\dagger[k], \end{aligned} \quad (28)$$

where the expectations are taken with respect to \mathbf{h}_{t,n_r} , $\mathbf{d}_{u,i}[k]$, and $\mathbf{d}_{d,j}[k]$, respectively. Denote the contributions of errors in (26), (27), and (28) through symmetric weight matrices $\mathbf{W}_{r,n_r} \succeq \mathbf{0}$, $\mathbf{W}_{u,i}[k] \succeq \mathbf{0}$, and $\mathbf{W}_{d,j}[k] \succeq \mathbf{0}$, respectively, in the weighted-sum mean-squared-error (WMSE) defined as

$$\begin{aligned} \Xi_{\text{wmse}} &\triangleq \underbrace{\sum_{k=1}^K \sum_{i=1}^I \alpha_i^u \text{Tr} \{ \mathbf{W}_{u,i}[k] \mathbf{E}_{u,i}[k] \}}_{=\Xi_{\text{UL}}} + \underbrace{\sum_{n_r=1}^{N_r} \alpha_{n_r}^r \text{Tr} \{ \mathbf{W}_{r,n_r} \mathbf{E}_{r,n_r} \}}_{=\Xi_r} \\ &+ \underbrace{\sum_{k=1}^K \sum_{j=1}^J \alpha_j^d \text{Tr} \{ \mathbf{W}_{d,j}[k] \mathbf{E}_{d,j}[k] \}}_{=\Xi_{\text{DL}}}. \end{aligned} \quad (29)$$

The $\mathbf{W}_{u,i}[k] \mathbf{E}_{u,i}[k]$, $\mathbf{W}_{d,j}[k] \mathbf{E}_{d,j}[k]$ and $\mathbf{W}_{r,n_r} \mathbf{E}_{r,n_r}$ used in the WMSE above are obtained in (30), (31) and (32) shown on top of the next page. Minimizing this WMSE is the key to solving a difficult non-convex problem in (25), as stated in the following theorem.

Theorem 1. *Solving the problem*

$$\begin{aligned} &\underset{\{\mathbf{P}\}, \{\mathbf{U}\}, \mathbf{A}, \{\mathbf{W}\}}{\text{minimize}} \quad \Xi_{\text{wmse}}(\{\mathbf{U}\}, \{\mathbf{P}\}, \mathbf{A}, \{\mathbf{W}\}), \\ &\text{subject to} \quad (24b) - (24d) \end{aligned} \quad (33)$$

yields the exact solution of the problem (25).

Proof: Using WMMSE optimization [31, 38], we solve (33) for $\{\mathbf{U}\}$ to obtain

$$\begin{aligned} \mathbf{U}_{r,n_r}^* &= \arg \min_{\mathbf{U}_{r,n_r}, \forall n_r} \text{Tr} \{ \mathbf{W}_{r,n_r} \mathbf{E}_{r,n_r} \} \\ &= \boldsymbol{\Sigma}_{t,n_r} \mathbf{S}_{t,n_r}^\dagger \left(\mathbf{S}_{t,n_r} \boldsymbol{\Sigma}_{t,n_r} \mathbf{S}_{t,n_r}^\dagger + \mathbf{R}_{\text{in},n_r} \right)^{-1}, \end{aligned} \quad (34)$$

$$\begin{aligned} \mathbf{U}_{u,i}^*[k] &= \arg \min_{\mathbf{U}_{u,i}[k], \forall i,k,l} \text{Tr} \{ \mathbf{W}_{u,i}[k] \mathbf{E}_{u,i}[k] \} \\ &= \mathbf{P}_{u,i}^\dagger[k] \mathbf{H}_{i,B} (\mathbf{R}_{i,B}^u[k,l])^{-1}, \end{aligned} \quad (35)$$

and

$$\begin{aligned} \mathbf{U}_{d,j}^*[k] &= \arg \min_{\mathbf{U}_{d,j}[k], \forall j,k,l} \text{Tr} \{ \mathbf{W}_{d,j}[k] \mathbf{E}_{d,j}[k] \} \\ &= \mathbf{P}_{d,j}^\dagger[k] \mathbf{H}_{B,j}^\dagger (\mathbf{R}_{j,B}^d[k])^{-1}. \end{aligned} \quad (36)$$

Substituting \mathbf{U}_{r,n_r}^* , $\mathbf{U}_{u,i}^*[k]$, and $\mathbf{U}_{d,j}^*[k]$ into MIs in (20)-(22) and MSEs in (26)-(28) yields, respectively, the achievable rates and minimum mean-squared-error (MMSE) of n_r^{th} radar Rx, i^{th} UL UE, and j^{th} DL UE as

$$R_{n_r}^r = \log \left| \mathbf{I} + \mathbf{S}_{t,n_r} \boldsymbol{\Sigma}_{t,n_r} \mathbf{S}_{t,n_r}^\dagger \mathbf{R}_{\text{in},n_r}^{-1} \right|, \quad (37a)$$

$$R_{u,i}[k] = \log \left| \mathbf{I} + \mathbf{R}_{i,B}[k] (\mathbf{R}_{\text{in},i}^u[k])^{-1} \right|, \quad (37b)$$

$$R_{d,j}[k] = \log \left| \mathbf{I} + \mathbf{R}_{B,j}[k] (\mathbf{R}_{\text{in},j}^d[k])^{-1} \right|, \quad (37c)$$

$$\mathbf{E}_{r,n_r}^* = \boldsymbol{\Sigma}_{t,n_r} \left[\mathbf{I} - \mathbf{S}_{t,n_r}^\dagger (\mathbf{R}_{\text{in},n_r}^r)^{-1} \mathbf{S}_{t,n_r} \boldsymbol{\Sigma}_{t,n_r} \right], \quad (37d)$$

$$\mathbf{E}_{i,B}^*[k] = \mathbf{I} - \mathbf{P}_{u,i}^\dagger[k] \mathbf{H}_{i,B}^\dagger (\mathbf{R}_{i,B}^u[k])^{-1} \mathbf{H}_{i,B} \mathbf{P}_{u,i}[k], \quad (37e)$$

and

$$\mathbf{E}_{B,j}^*[k] = \mathbf{I} - \mathbf{P}_{d,j}^\dagger[k] \mathbf{H}_{B,j}^\dagger (\mathbf{R}_{d,j}[k])^{-1} \mathbf{H}_{B,j} \mathbf{P}_{d,j}[k]. \quad (37f)$$

Recall the *data processing inequality* [40, p.34] which implies that $R_{n_r}^r$, $R_{u,i}[k]$, and $R_{d,j}[k]$ are the upper bounds of $I_{n_r}^r$, $I_i^u[k]$, and $I_j^d[k]$, for all n_r , i , and j . It follows that $\{\mathbf{U}^*\} \triangleq$

$$\begin{aligned} \mathbf{W}_{u,i}[k]\mathbf{E}_{u,i}[k] &= \mathbf{W}_{u,i}[k]\mathbf{I} - 2\mathbf{W}_{u,i}[k]\mathbf{U}_{u,i}[k]\mathbf{H}_{i,B}\mathbf{P}_{u,i}[k] + \mathbf{W}_{u,i}[k]\mathbf{U}_{u,i}[k]\mathbf{H}_{i,B}\mathbf{P}_{u,i}[k]\mathbf{P}_{u,i}^\dagger[k]\mathbf{H}_{i,B}^\dagger\mathbf{U}_{u,i}[k] \\ &+ \mathbf{W}_{u,i}[k]\mathbf{U}_{u,i}[k] \left(\sum_{q \neq i} \mathbf{H}_{q,B}\mathbf{P}_{u,q}[k]\mathbf{P}_{u,q}^\dagger[k]\mathbf{H}_{q,B}^\dagger + \sum_{j=1}^J \mathbf{H}_{BB}\mathbf{P}_{d,j}[k]\mathbf{P}_{d,j}^\dagger[k]\mathbf{H}_{BB}^\dagger + \mathbf{H}_{rB}\mathbf{a}[k]\mathbf{a}^\dagger[k]\mathbf{H}_{rB}^\dagger \right) \mathbf{U}_{u,i}^\dagger[k], \quad (30) \end{aligned}$$

$$\begin{aligned} \mathbf{W}_{d,j}[k]\mathbf{E}_{d,j}[k] &= \mathbf{W}_{d,j}[k]\mathbf{I} - 2\mathbf{W}_{u,i}[k]\mathbf{U}_{d,j}[k]\mathbf{H}_{B,j}\mathbf{P}_{d,j}[k] + \mathbf{W}_{d,j}[k]\mathbf{U}_{d,j}[k]\mathbf{H}_{B,j}\mathbf{P}_{d,j}[k]\mathbf{P}_{d,j}^\dagger[k]\mathbf{H}_{B,j}^\dagger\mathbf{U}_{d,j}^\dagger[k] \\ &+ \mathbf{W}_{d,j}[k]\mathbf{U}_{d,j}[k] \left(\sum_{g \neq j} \mathbf{H}_{B,j}\mathbf{P}_{u,g}[k]\mathbf{P}_{u,g}^\dagger[k]\mathbf{H}_{B,j}^\dagger + \sum_{i=1}^I \mathbf{H}_{i,j}\mathbf{P}_{u,i}[k]\mathbf{P}_{u,i}^\dagger[k]\mathbf{H}_{i,j}^\dagger + \mathbf{H}_{r,j}\mathbf{a}[k]\mathbf{a}^\dagger[k]\mathbf{H}_{r,j}^\dagger \right) \mathbf{U}_{d,j}^\dagger[k], \quad (31) \end{aligned}$$

$$\begin{aligned} \text{and } \mathbf{W}_{r,n_r}\mathbf{E}_{r,n_r} &= \mathbf{W}_{r,n_r}\mathbb{E} \left[\left(\mathbf{h}_{t,n_r} - \sum_{k=1}^K \mathbf{u}_{r,n_r}[k] \{ \mathbf{y}_{t,n_r}^\dagger[k] + \mathbf{y}_{in,n_r}[k] \} \right) \left(\mathbf{h}_{t,n_r} - \sum_{k=1}^K \mathbf{u}_{r,n_r}[k] \{ \mathbf{y}_{t,n_r}^\dagger[k] + \mathbf{y}_{in,n_r}[k] \} \right)^\dagger \right] \\ &= \mathbf{W}_{r,n_r}\boldsymbol{\Sigma}_{t,n_r} - 2\mathbf{W}_{r,n_r} \sum_{k=1}^K \mathbf{u}_{r,n_r}[k] \mathbf{s}_{t,n_r}^\top[k] \boldsymbol{\Sigma}_{t,n_r} + \mathbf{W}_{r,n_r} \sum_{m=1}^K \sum_{\ell=1}^K \mathbf{u}_{r,n_r}[m] \mathbf{s}_{t,n_r}^\top[m] \boldsymbol{\Sigma}_{t,n_r} \mathbf{s}_{t,n_r}^*[m] \mathbf{u}_{r,n_r}^\dagger[\ell] \\ &+ \mathbf{W}_{r,n_r} \sum_{m=1}^K \sum_{\ell=1}^K \mathbf{u}_{r,n_r}[m] (\mathbf{R}_{Bm,n_r}(m,\ell) + \mathbf{R}_{U,n_r}(m,\ell) + \mathbf{R}_{c,n_r}(m,\ell) + \sigma_{n_r}) \mathbf{u}_{r,n_r}^\dagger[\ell]. \quad (32) \end{aligned}$$

$\{\mathbf{U}_{r,n_r}^*, \mathbf{U}_{u,i}^*[k], \mathbf{U}_{d,j}^*[k], \forall \{n_r, i, j\}\}$ is also the optimal solution of (25) and, in turn, the original problem (24), whose additional constraints do not affect the solution for $\{\mathbf{U}\}$.

Using the Woodbury matrix identity [49], the achievable rate is related to the MMSE matrix as $R_{u,i}[k] = \log \left| (\mathbf{E}_{i,B}^*[k])^{-1} \right|$, $R_{d,j}[k] = \log \left| (\mathbf{E}_{B,j}^*[k])^{-1} \right|$, and $R_{r,n_r}^r = \log \left| \boldsymbol{\Sigma}_{t,n_r} (\mathbf{E}_{r,n_r}^*)^{-1} \right|$. Define

$$\begin{aligned} \Xi'_{\text{wmse}} &= \Xi_{\text{wmse}} - \sum_{n_r=1}^{N_r} \alpha_{n_r}^r (\boldsymbol{\Sigma}_{t,n_r} \log |\mathbf{W}_{r,n_r}| + M) - \\ &\sum_{k=1}^K \left\{ \sum_{i=1}^I \alpha_i^u (\log |\mathbf{W}_{u,i}[k]| + D_i^u) + \sum_{j=1}^J \alpha_j^d (\log |\mathbf{W}_{d,j}[k]| + D_j^d) \right\}. \end{aligned}$$

Applying the first order optimal condition [50] with respect to $\{\mathbf{W}\}$ produces the optimal weight matrices $\{\mathbf{W}^*\}$ as $\mathbf{W}_{u,i}^*[k] = (\mathbf{E}_{u,i}[k])^{-1}$, $\mathbf{W}_{d,j}^*[k] = (\mathbf{E}_{d,j}[k])^{-1}$, and $\mathbf{W}_{r,n_r}^* = (\mathbf{E}_{r,n_r})^{-1}$ for all $\{n_r, i, j\}$. Substituting $\{\mathbf{W}^*\}$ and $\{\mathbf{U}^*\}$ in Ξ'_{wmse} results in

$$\begin{aligned} \Xi'_{\text{wmse}} &= \sum_{k=1}^K \left\{ - \sum_{j=1}^J \alpha_j^d \log \left| (\mathbf{E}_{B,j}^*[k])^{-1} \right| \right. \\ &- \left. \sum_{i=1}^I \alpha_i^u \log \left| (\mathbf{E}_{i,B}^*[k])^{-1} \right| \right\} - \alpha_r \sum_{n_r=1}^{N_r} \log \left| (\mathbf{E}_{r,n_r}^*)^{-1} \right| \\ &= \sum_{k=1}^K \left\{ \sum_{j=1}^J \alpha_j^d R_{d,j}[k] + \sum_{i=1}^I \alpha_i^u R_{u,i}[k] \right\} + \sum_{n_r=1}^{N_r} \alpha_{n_r}^r R_{r,n_r}, \quad (38) \end{aligned}$$

which leads to

$$\Xi'_{\text{wmse}}(\{\mathbf{U}^*\}, \{\mathbf{W}^*\}, \{\mathbf{P}\}, \mathbf{A}) = -I_{\text{CWSM}}(\{\mathbf{U}^*\}, \{\mathbf{P}\}, \mathbf{A}). \quad (39)$$

This demonstrates that maximizing I_{CWSM} is equal to minimizing Ξ'_{wmse} using the WMMSE receive filters $\{\mathbf{U}^*\}$. Since only Ξ_{wmse} depends on $\{\mathbf{P}\}$ and \mathbf{A} , minimizing Ξ'_{wmse} is equivalent to maximizing I_{CWSM} with respect to $\{\mathbf{P}\}$ and \mathbf{A} . This completes the proof. \blacksquare

Define $\text{WMMSE}, \Xi_{\text{wmmse}}(\{\mathbf{P}\}, \mathbf{A}) \triangleq \Xi_{\text{wmse}}(\{\mathbf{U}^*\}, \{\mathbf{W}^*\}, \{\mathbf{P}\}, \mathbf{A})$. Substituting $\{\mathbf{U}^*\}$ and $\{\mathbf{W}^*\}$, the problem in (33) becomes

$$\underset{\{\mathbf{P}\}, \mathbf{A}}{\text{minimize}} \Xi_{\text{wmmse}}(\{\mathbf{P}\}, \mathbf{A}) \text{ subject to } (24b) - (24d). \quad (40)$$

As explained next, we address this problem using coordinate descent.

B. WMMSE-MRMC

In order to solve (40), we iterate over all UL precoders $\mathbf{P}_{u,i}[k]$ for $i \in \mathbb{Z}_+ \{I\}$, DL precoders $\mathbf{P}_{d,j}[k]$ for $j \in \mathbb{Z}_+ \{J\}$, and the radar code vectors $\mathbf{a}[k]$ for $k \in \mathbb{Z}_+ \{K\}$, using the Lagrange dual method to find a closed form solution to each variable. These steps constitutes our WMMSE-MRMC algorithm.

1) *Lagrange dual solution:* Denote the Lagrange multiplier vectors with respect to constraints (24b)-(24d), respectively, as $\boldsymbol{\lambda}_{\text{DL}} \triangleq [\lambda_d[1], \dots, \lambda_d[K]]^\top$, $\boldsymbol{\lambda}_{\text{UL}} \triangleq [\lambda_{u,1}[1], \dots, \lambda_{u,I}[K]]^\top$, $\boldsymbol{\mu}_{\text{DL}} \triangleq [\mu_{d,1}[1], \dots, \mu_{d,J}[K]]^\top$, and $\boldsymbol{\mu}_{\text{UL}} \triangleq [\mu_{u,1}[1], \dots, \mu_{u,I}[K]]^\top$. Define UL power vector $\mathbf{p}_{\text{UL}} \triangleq [P_{u,1}[1], \dots, P_{u,I}[K]]^\top$, DL power vector $\mathbf{p}_{\text{DL}} \triangleq [\sum_{j=1}^J P_{d,j}[1], \dots, \sum_{j=1}^J P_{d,j}[K]]^\top$, $\mathbf{r}_{\text{UL}} \triangleq$, UL rate vector $[R_{u,1}[1], \dots, R_{u,I}[K]]^\top$, and DL rate vector $\mathbf{r}_{\text{DL}} \triangleq [R_{d,1}[1], \dots, R_{d,J}[K]]^\top$. The Lagrangian associated with (40) is

$$\begin{aligned} \mathcal{L}(\{\mathbf{P}\}, \mathbf{A}, \boldsymbol{\lambda}, \boldsymbol{\mu}) &= \Xi_{\text{wmmse}} + \boldsymbol{\lambda}_{\text{DL}}^\top (\mathbf{p}_{\text{DL}} - P_{\text{B}}\mathbf{1}) + \boldsymbol{\lambda}_{\text{UL}}^\top (\mathbf{p}_{\text{UL}} - P_{\text{U}}\mathbf{1}) \\ &- \boldsymbol{\mu}_{\text{DL}}^\top (\mathbf{r}_{\text{DL}} - R_{\text{DL}}\mathbf{1}) - \boldsymbol{\mu}_{\text{UL}}^\top (\mathbf{r}_{\text{UL}} - R_{\text{UL}}\mathbf{1}). \quad (41) \end{aligned}$$

Define $\boldsymbol{\lambda} = [\boldsymbol{\lambda}_{\text{DL}}^\top, \boldsymbol{\lambda}_{\text{UL}}^\top]^\top$ and $\boldsymbol{\mu} = [\boldsymbol{\mu}_{\text{DL}}^\top, \boldsymbol{\mu}_{\text{UL}}^\top]^\top$. The Lagrange dual function of $L(\cdot)$ is $D(\boldsymbol{\lambda}, \boldsymbol{\mu}) = \inf_{\{\mathbf{P}\}, \mathbf{A}} \mathcal{L}(\{\mathbf{P}\}, \mathbf{A}, \boldsymbol{\lambda}, \boldsymbol{\mu})$. With these definitions, we state the following theorem to solve (40).

Theorem 2. *Linearize, using Taylor series approximation, $R_{u,i}[k]$ and $R_{d,j}[k]$, $\forall \{i, j, k\}$ in the QoS constraints of problem (40). Then, the solution of the resulting problem is equivalent to that of its Lagrange dual problem*

$$\text{maximize } D(\boldsymbol{\lambda}, \boldsymbol{\mu}) \text{ subject to } \boldsymbol{\lambda} \succeq \mathbf{0}, \boldsymbol{\mu} \succeq \mathbf{0}. \quad (42)$$

Proof: See Appendix A. \blacksquare

Next, we find closed form solutions to $\mathbf{P}_{u,i}[k]$, $\mathbf{P}_{d,j}[k]$, and $\mathbf{a}[k]$. From Appendix B, the gradients of Lagrangian $\mathcal{L}(\cdot)$ with respect to $\mathbf{P}_{u,i}[k]$, $\mathbf{P}_{d,j}[k]$, and $\mathbf{a}[k]$ are, respectively,

$$\begin{aligned} \nabla_{\mathbf{P}_{u,i}[k]} \mathcal{L} &= \nabla_{\mathbf{P}_{u,i}[k]} \Xi_{\text{UL}} + \nabla_{\mathbf{P}_{u,i}[k]} \Xi_{\text{DL}} + \nabla_{\mathbf{P}_{u,i}[k]} \Xi_r + \lambda_{u,i}[k] \mathbf{P}_{u,i}[k] \\ &- \sum_{g=1}^J \mu_{u,g}[k] \nabla_{\mathbf{P}_{u,i}[k]} R_{d,g}[k] - \sum_{q=1}^I \mu_{u,q}[k] \nabla_{\mathbf{P}_{u,i}[k]} R_{u,q}[k], \\ \nabla_{\mathbf{P}_{d,j}[k]} \mathcal{L} &= \nabla_{\mathbf{P}_{d,j}[k]} \Xi_{\text{UL}} + \nabla_{\mathbf{P}_{d,j}[k]} \Xi_{\text{DL}} + \nabla_{\mathbf{P}_{d,j}[k]} \Xi_r + \lambda_d[k] \mathbf{P}_{d,j}[k] \\ &- \sum_{g=1}^J \mu_{u,g}[k] \nabla_{\mathbf{P}_{d,j}[k]} R_{d,g}[k] - \sum_{q=1}^I \mu_{u,q}[k] \nabla_{\mathbf{P}_{d,j}[k]} R_{u,q}[k], \end{aligned}$$

and

$$\begin{aligned} \nabla_{\mathbf{a}[k]} \mathcal{L} &= \nabla_{\mathbf{a}[k]} \Xi_{\text{UL}} + \nabla_{\mathbf{a}[k]} \Xi_{\text{DL}} + \nabla_{\mathbf{a}[k]} \Xi_r, \\ &- \sum_{j=1}^J \mu_{d,j}[k] \nabla_{\mathbf{a}[k]} R_{d,j}[k] - \sum_{i=1}^I \mu_{u,i}[k] \nabla_{\mathbf{a}[k]} R_{u,i}[k]. \end{aligned}$$

The closed form solutions to $\mathbf{P}_{u,i}^*[k]$, $\mathbf{P}_{d,j}^*[k]$, and $\mathbf{a}'[k]$ are obtained by solving equations $\nabla_{\mathbf{P}_{u,i}[k]} \mathcal{L} = 0$, $\nabla_{\mathbf{P}_{d,j}[k]} \mathcal{L} = 0$, and $\nabla_{\mathbf{a}'[k]} \mathcal{L} = 0$, respectively. After some algebraic computations on the aforementioned equations and using $\boldsymbol{\xi}_{\text{UL}}[k]$ and $\boldsymbol{\xi}_{d,g}[k]$ from Appendix B, we obtain three Sylvester equations $\mathbf{A}_{u,i}[k] \mathbf{P}_{u,i}^*[k] + \mathbf{P}_{u,i}^*[k] \mathbf{B}_{u,i}[k] = \mathbf{C}_{u,i}[k]$, $\mathbf{A}_{d,j}[k] \mathbf{P}_{d,j}^*[k] + \mathbf{P}_{d,j}^*[k] \mathbf{B}_{d,j}[k] = \mathbf{C}_{d,j}[k]$, and $\mathbf{A}_r[k] \mathbf{a}'[k] + \mathbf{a}'[k] \mathbf{B}_r[k] = \mathbf{C}_r[k]$, where

$$\begin{aligned}
\mathbf{A}_{u,i}[k] &= \mathbf{H}_{i,B}^\dagger \boldsymbol{\xi}_{UL}[k] \mathbf{H}_{i,B} + \sum_{g=1}^J \mathbf{H}_{i,g}^\dagger \boldsymbol{\xi}_{d,g}[k] \mathbf{H}_{i,g} + \lambda_{u,i}[k] \mathbf{I}, \\
\mathbf{B}_{u,i}[k] &= \sum_{n_r=1}^{N_r} \eta_{i,n_r}^2 \mathbf{d}_{u,i}[k] \xi_{n_r}(k, k) \mathbf{d}_{u,i}^\dagger[k], \\
\mathbf{C}_{u,i}[k] &= \sum_{q=1}^I \mu_{u,q}[k] \nabla_{\mathbf{P}_{u,i}[k]} R_{u,q}[k] + \sum_{g=1}^J \mu_{u,g}[k] \nabla_{\mathbf{P}_{u,i}[k]} R_{d,g}[k] \\
&\quad - \sum_{n_r=1}^{N_r} \eta_{i,n_r}^2 \sum_{m \neq k}^K \mathbf{P}_{u,i}[m] \mathbf{d}_{u,i}[m] \xi_{n_r}(m, k) \mathbf{d}_{u,i}^\dagger[k], \\
\mathbf{A}_{d,j}[k] &= \mathbf{H}_{BB}^\dagger \boldsymbol{\xi}_{UL}[k] \mathbf{H}_{BB} + \sum_{g=1}^J \mathbf{H}_{B,g}^\dagger \boldsymbol{\xi}_{d,g}[k] \mathbf{H}_{B,g} + \lambda_d[k] \mathbf{I}, \\
\mathbf{B}_{d,j}[k] &= \sum_{n_r=1}^{N_r} \eta_{Bt,n_r}^2 \mathbf{d}_{d,j}[k] \xi_{n_r}(k, k) \mathbf{d}_{d,j}^\dagger[k], \\
&\quad + \sum_{n_r=1}^{N_r} \mathbf{d}_{d,j}[k] \xi_{n_r}(k, k) \mathbf{d}_{d,j}^\dagger[k], \\
\mathbf{C}_{d,j}[k] &= \sum_{q=1}^I \mu_{u,q}[k] \nabla_{\mathbf{P}_{d,j}[k]} R_{u,q}[k] + \sum_{g=1}^J \mu_{u,g}[k] \nabla_{\mathbf{P}_{d,j}[k]} R_{d,g}[k] \\
&\quad - \sum_{n_r=1}^{N_r} \mathbf{J}_{Bt,n_r}^\top \sum_{m=1}^K \mathbf{s}_{t,n_r}[m] \xi_{n_r}(m, k) \mathbf{d}_{d,j}^\dagger[k] \\
&\quad - \sum_{n_r=1}^{N_r} \sum_{m \neq k}^K \sum_{g=1}^J \mathbf{P}_{d,g}[m] \mathbf{d}_{d,g}[m] \xi_{n_r}(m, k) \eta_{Bm,n_r}^2 \mathbf{d}_{d,j}^\dagger[k] \\
&\quad - \sum_{n_r=1}^{N_r} \sum_{g \neq j}^J \mathbf{P}_{d,g}[k] \mathbf{d}_{d,g}[k] \xi_{n_r}(k, k) \eta_{Bm,n_r}^2 \mathbf{d}_{d,j}^\dagger[k], \\
\mathbf{A}_r[k] &= \mathbf{H}_{rB}^\dagger \boldsymbol{\xi}_{UL}[k] \mathbf{H}_{rB} + \sum_{j=1}^J \mathbf{H}_{r,j}^\dagger \boldsymbol{\xi}_{d,j}[k] \mathbf{H}_{r,j}, \\
\mathbf{B}_r[k] &= \sum_{n_r=1}^{N_r} \eta_{n_r,n_r}^2 \xi_{n_r}(k, k), \\
\text{and } \mathbf{C}_r[k] &= \sum_{i=1}^I \mu_{u,i}[k] \nabla_{\mathbf{a}[k]} R_{u,i}[k] + \sum_{j=1}^J \mu_{d,j}[k] \nabla_{\mathbf{a}[k]} R_{d,j}[k] \\
&\quad - \sum_{n_r=1}^{N_r} \mathbf{Q}_{r,n_r}^\dagger[k] \mathbf{J}_r^\top \sum_{m \neq k}^K \mathbf{s}_{t,n_r}[m] \xi_{n_r}(m, k).
\end{aligned}$$

The solutions to these Sylvester equations with respect to $\mathbf{P}_{u,i}^*[k]$, $\mathbf{P}_{d,j}^*[k]$, and $\mathbf{a}'[k]$ are obtained as [49]

$$\text{vec}(\mathbf{P}_{u,i}^*[k]) = (\mathbf{I} \otimes \mathbf{A}_{u,i}[k] + \mathbf{B}_{u,i}^\top[k] \otimes \mathbf{I})^{-1} \text{vec}(\mathbf{C}_{u,i}[k]), \quad (44a)$$

$$\text{vec}(\mathbf{P}_{d,j}^*[k]) = (\mathbf{I} \otimes \mathbf{A}_{d,j}[k] + \mathbf{B}_{d,j}^\top[k] \otimes \mathbf{I})^{-1} \text{vec}(\mathbf{C}_{d,j}[k]), \quad (44b)$$

$$\text{and } \mathbf{a}'[k] = [\mathbf{I} \otimes \mathbf{A}_r[k] + \mathbf{B}_r^\top[k] \otimes \mathbf{I}]^{-1} \mathbf{C}_r[k], \quad \forall i, j, k. \quad (44c)$$

In order to determine $\mathbf{P}_{u,i}^*[k]$, $\mathbf{P}_{d,j}^*[k]$, and $\mathbf{a}'[k]$, we need to find the optimal $\boldsymbol{\lambda}^*$ and $\boldsymbol{\mu}^*$.

2) *Subgradient method for precoders:* We employ the sub-gradient method [50] to find $\boldsymbol{\lambda}^*$ and $\boldsymbol{\mu}^*$ sequentially, where at the t^{th} iteration, the updated values are [42]

$$\lambda_{u,i}^{(t+1)}[k] = \left[\lambda_{u,i}^{(t)}[k] + \beta_{u,i}^{(t)}[k] \left(\text{Tr} \left\{ \mathbf{P}_{u,i}^{(t)}[k] \left(\mathbf{P}_{u,i}^{(t)}[k] \right)^\dagger \right\} - P_U \right) \right]^+, \quad (45a)$$

$$\lambda_d^{(t+1)}[k] = \left[\lambda_d^{(t)}[k] + \beta_d^{(t)}[k] \left(\sum_{j=1}^J \text{Tr} \left\{ \mathbf{P}_{d,j}^{(t)}[k] \left(\mathbf{P}_{d,j}^{(t)}[k] \right)^\dagger \right\} - P_B \right) \right]^+, \quad (45b)$$

$$\mu_{u,i}^{(t+1)}[k] = \left[\mu_{u,i}^{(t)}[k] + \varepsilon_{u,i}^{(t)}[k] \left(R_{UL} - R_{u,i}^{(t)}[k] \right) \right]^+, \quad (45c)$$

and

$$\mu_{d,j}^{(t+1)}[k] = \left[\mu_{d,j}^{(t)}[k] + \varepsilon_{d,j}^{(t)}[k] \left(R_{DL} - R_{d,j}^{(t)}[k] \right) \right]^+, \quad (45d)$$

where $\beta_{u,i}^{(t)}[k] \triangleq 1/t$, $\beta_d^{(t)}[k] \triangleq 1/t$, $\varepsilon_{u,i}^{(t)}[k] \triangleq 1/t$, and $\varepsilon_{d,j}^{(t)}[k] \triangleq 1/t$ denote the step sizes of the t^{th} iteration for $\lambda_{u,i}^{(t)}[k]$, $\lambda_d^{(t)}[k]$, $\mu_{u,i}^{(t)}[k]$, and $\mu_{d,j}^{(t)}[k]$, respectively, $\mathbf{P}_{u,i}^{(t)}[k]$, $\mathbf{P}_{d,j}^{(t)}[k]$, $R_{u,i}^{(t)}[k]$, $R_{d,j}^{(t)}[k]$, and $\Xi_{\text{wmmse}}^{(t)}$ the t^{th} iterates of $\mathbf{P}_{u,i}[k]$, $\mathbf{P}_{d,j}[k]$, $R_{u,i}[k]$, $R_{d,j}[k]$, and Ξ_{wmmse} , respectively. Note that $\mathbf{P}_{u,i}^{(t)}[k]$ and $\mathbf{P}_{d,j}^{(t)}[k]$ are obtained by replacing $\lambda_{u,i}[k]$ and $\mu_{u,i}[k]$ with $\lambda_{u,i}^{(t)}[k]$ and $\mu_{u,i}^{(t)}[k]$ in (44a) as well as $\lambda_d[k]$ and $\mu_{d,j}[k]$ with $\lambda_d^{(t)}[k]$ and $\mu_{d,j}^{(t)}[k]$ in (44b), respectively.

Algorithms 1 and 2 summarize the steps of sub-gradient based algorithms to find $\boldsymbol{\lambda}^*$ and $\boldsymbol{\mu}^*$, respectively. Here, $(\cdot)^{(\ell, \iota, t)}$ denotes the iterate of a variable at the ℓ^{th} , ι^{th} , and t^{th} iterations of BCD-AP MRMC, WMMSE-MRMC and subgradient algorithms. The variables $t_{u,\max}$ and $t_{d,\max}$ denote the maximum iterations and $\left\{ \mathbf{P}^{(\ell, \iota, 0)} \right\} \triangleq \left\{ \mathbf{P}_{u,i}^{(\ell, \iota, 0)}[k], \mathbf{P}_{d,j}^{(\ell, \iota, 0)}[k], \forall \{i, j, k\} \right\}$. As the sub-gradient method is not descent-based and $\Xi_{\text{wmmse}}^{(t)}$ may increase at certain iterations [42], $\lambda_{u,i}^*[k]$, $\mu_{u,i}^*[k]$, $\lambda_d^*[k]$, and $\mu_{d,j}^*[k]$ are employed to keep track of $\lambda_{u,i}^{(t)}[k]$, $\mu_{u,i}^{(t)}[k]$, $\lambda_d^{(t)}[k]$, and $\mu_{d,j}^{(t)}[k]$, that yield the minimum $\Xi_{\text{wmmse}}^{(t)}$ in the current iteration, i.e. $\Xi_{\text{wmmse}}^{\min}$.

Algorithm 1 Subgradient approach to solve (42) for UL UE

Input: $\left\{ \mathbf{P}^{(\ell, \iota)} \right\}$, $\mathbf{A}^{(\ell, \iota)}$, $\left\{ \mathbf{U}^{(\ell)} \right\}$, $t_{u,\max}$
Output: $\mathbf{P}_{u,i}^{(\ell, \iota)}[k]$, $\mu_{u,i}^*[k]$

- 1: Initialize $\lambda_{u,i}^{(0)}[k] = 1$, $\mu_{u,i}^{(0)}[k] = 1$, $\left\{ \mathbf{P}^{(\ell, \iota, 0)} \right\} = \left\{ \mathbf{P}^{(\ell, \iota)} \right\}$
- 2: $\Xi_{\text{wmmse}}^{(0)}$, $R_{u,i}^{(0)}[k] \leftarrow^{(29), (37b)} \left\{ \mathbf{P}^{(\ell, \iota)} \right\}$, $\mathbf{A}^{(\ell, \iota)}$, $\left\{ \mathbf{U}^{(\ell)} \right\}$
- 3: Set the iteration index $t = 1$
- 4: **repeat**
- 5: $\left\{ \mathbf{P}^{(\ell, \iota, t)} \right\} \leftarrow \left\{ \mathbf{P}^{(\ell, \iota, t-1)} \right\}$, $\beta_{u,i}^{(t)}[k] \leftarrow 1/t$, $\varepsilon_{u,i}^{(t)}[k] \leftarrow 1/t$
- 6: Update $\lambda_{u,i}^{(t)}[k]$ via (45a) with $\mathbf{P}_{u,i}^{(\ell, \iota, t-1)}[k]$ and $\lambda_{u,i}^{(t-1)}[k]$, $\mu_{u,i}^{(t)}[k]$ via (45c) with $\beta_{u,i}^{(t-1)}[k]$ and $R_{u,i}^{(t-1)}[k]$,
- 7: Set $\tilde{\mathbf{P}}_{u,i}[k] = \mathbf{P}_{u,i}^{(\ell, \iota, t-1)}[k]$; update $\mathbf{P}_{u,i}^{(\ell, \iota, t)}[k]$ via (44a) with $\lambda_{u,i}^{(t)}[k]$, $\mu_{u,i}^{(t)}[k]$, $\left\{ \tilde{\mathbf{P}} \right\}$, $\left\{ \mathbf{P}^{(\ell, \iota, t)} \right\}$, $\mathbf{A}^{(\ell, \iota)}$, $\left\{ \mathbf{U}^{(\ell)} \right\}$
- 8: Update $\Xi_{\text{wmmse}}^{(t)}$ via (29) with $\left\{ \mathbf{P}^{(\ell, \iota, t)} \right\}$, $\mathbf{A}^{(\ell, \iota)}$, $\left\{ \mathbf{U}^{(\ell)} \right\}$
- 9: **if** $\Xi_{\text{wmmse}}^{(t)} > \Xi_{\text{wmmse}}^{\min}$ **then** $\mathbf{P}_{u,i}^{(\ell, \iota)}[k] = \mathbf{P}_{u,i}^{(\ell, \iota, t)}[k]$, $\lambda_{u,i}^*[k] = \lambda_{u,i}^{(t)}[k]$, $\mu_{u,i}^*[k] = \mu_{u,i}^{(t)}[k]$, and $\Xi_{\text{wmmse}}^{\min} = \Xi_{\text{wmmse}}^{(t)}$
- 10: Update $R_{u,i}^{(t)}[k]$ with $\left\{ \mathbf{P}^{(\ell, \iota, t)} \right\}$ from (37b)
- 11: $t \leftarrow t + 1$
- 12: **until** $t > t_{u,\max}$
- 13: **return** $\mathbf{P}_{u,i}^{(\ell, \iota)}[k]$, $\mu_{u,i}^*[k]$

During the ℓ^{th} iteration of the BCD-AP MRMC algorithm (Algorithm 5) and the ι^{th} iteration of the WMMSE-MRMC algorithm (Algorithm 3), upon executing Algorithms 1 and 2 for all i, j , and k , $\mathbf{A}^{(\ell, \iota)}$ can be solved by replacing $\boldsymbol{\mu}^*$ and $\left\{ \mathbf{P}^{(\ell, \iota)} \right\}$ with $\boldsymbol{\mu}$ and $\left\{ \mathbf{P} \right\}$ in (44c). The output of the WMMSE-MRMC algorithm outputs the ℓ^{th} iterate of the precoders $\left\{ \mathbf{P}^{(\ell)} \right\}$ of the BCD-AP MRMC algorithm as well as \mathbf{A}' . The number of iterations for WMMSE-MRMC is limited to t_{\max} .

*C. Nearest vector method to find \mathbf{A}^**

Upon obtaining $\mathbf{A}' = [\mathbf{a}'_1, \dots, \mathbf{a}'_{M_r}]$, which is the optimal solution for $\mathbf{A} \subseteq \mathbb{A}_c$, the next step in BCD-AP algorithm is to apply AP for projecting \mathbf{a}'_{m_r} onto \mathbb{A}_r . The nearest element of \mathbf{a}'_{m_r} in \mathbb{A}_r for all m_r in the following problem

Algorithm 2 Subgradient approach to solve (42) for DL UE

Input: $\{\mathbf{P}^{(\ell,\iota)}\}$, $\mathbf{A}^{(\ell,\iota)}$, $\{\mathbf{U}^{(\ell)}\}$, $t_{d,\max}$

Output: $\mathbf{P}_{d,j}^{(\ell,\iota)}[k]$, $\mu_{d,j}^*[k]$

- 1: Initialize $\lambda_d^{(0)}[k] = 1$, $\mu_{d,j}^{(0)}[k] = 1$, and $\{\mathbf{P}^{(\ell,\iota,0)}\} = \{\mathbf{P}^{(\ell,\iota)}\}$
- 2: $\Xi_{\text{wmmse}}^{(0)}$, $R_{d,j}^{(0)}[k] \leftarrow^{(29),(37c)} \{\mathbf{P}^{(\ell,\iota)}\}$, $\mathbf{A}^{(\ell,\iota)}$, $\{\mathbf{U}^{(\ell)}\}$
- 3: Set the iteration index $t = 1$
- 4: **repeat**
- 5: $\{\mathbf{P}^{(\ell,\iota,t)}\} \leftarrow \{\mathbf{P}^{(\ell,\iota,t-1)}\}$, $\beta_{d,j}^{(t)}[k] \leftarrow 1/t$, $\varepsilon_{d,j}^{(t)}[k] \leftarrow 1/t$
- 6: Update $\lambda_d^{(t)}[k]$ via (45b) with $\mathbf{P}_{d,j}^{(\ell,\iota,t-1)}[k]$ and $\lambda_d^{(t-1)}[k]$, $\mu_{d,j}^{(t)}[k]$ via (45d) with $\beta_{d,j}^{(t-1)}[k]$ and $R_{d,j}^{(t-1)}[k]$,
- 7: Set $\tilde{\mathbf{P}}_{d,j}[k] = \mathbf{P}_{d,j}^{(\ell,\iota,t-1)}[k]$; update $\mathbf{P}_{d,j}^{(\ell,\iota,t)}[k]$ via (44b) with $\lambda_d^{(t)}[k]$, $\mu_{d,j}^{(t)}[k]$, $\{\tilde{\mathbf{P}}\}$, $\{\mathbf{P}^{(\ell,\iota,t)}\}$, $\mathbf{A}^{(\ell,\iota)}$, $\{\mathbf{U}^{(\ell)}\}$
- 8: Update $\Xi_{\text{wmmse}}^{(t)}$ via (29) with $\{\mathbf{P}^{(\ell,\iota,t)}\}$, $\mathbf{A}^{(\ell,\iota)}$, $\{\mathbf{U}^{(\ell)}\}$
- 9: **if** $\Xi_{\text{wmmse}}^{(t)} \geq \Xi_{\text{wmmse}}^{(t-1)}$ **then** $\mathbf{P}_{d,j}^{(\ell,\iota,t)}[k] = \mathbf{P}_{d,j}^{(\ell,\iota,t-1)}[k]$, $\mu_{d,j}^*[k] = \mu_{d,j}^{(t-1)}[k]$, and $\Xi_{\text{wmmse}}^{\min} = \Xi_{\text{wmmse}}^{(t-1)}$
- 10: Update $R_{d,j}^{(t)}[k]$ with $\{\mathbf{P}^{(\ell,\iota,t)}\}$ from (37c)
- 11: $t \leftarrow t + 1$
- 12: **until** $t > t_{d,\max}$
- 13: **return** $\mathbf{P}_{d,j}^{(\ell,\iota)}[k]$, $\mu_{d,j}^*[k]$

Algorithm 3 WMMSE-MRMC algorithm to solve (40)

Input: $\{\mathbf{P}^{(\ell)}\}$, $\mathbf{A}^{(\ell)}$, $\{\mathbf{U}^{(\ell)}\}$, ℓ_{\max} , $t_{u,\max}$, and $t_{d,\max}$

Output: $\{\mathbf{P}^{(\ell)}\}$, \mathbf{A}'

- 1: Set $\{\mathbf{P}^{(\ell,0)}\} \triangleq \{\mathbf{P}_{u,i}^{(\ell,0)}[k], \mathbf{P}_{d,j}^{(\ell,0)}[k], \forall \{i, j, k\}\} = \{\mathbf{P}^{(\ell)}\}$ and $\mathbf{A}^{(\ell,0)} \triangleq \left[\left(\mathbf{a}^{(\ell,0)}[1] \right)^\top; \dots; \left(\mathbf{a}^{(\ell,0)}[K] \right)^\top \right] = \mathbf{A}^{(\ell)}$
- 2: Set the iteration index $\iota = 0$
- 3: **repeat**
- 4: **for** $k = 1, \dots, K$ **do**
- 5: **for** $i = 1, \dots, I$ **do**
- 6: $\mathbf{P}_{u,i}^{(\ell,\iota+1)}[k], \mu_{u,i}^*[k] \leftarrow^{\frac{\text{Algorithm 1}}{t_{u,\max}}} \{\mathbf{P}^{(\ell,\iota)}\}, \mathbf{A}^{(\ell,\iota)}, \{\mathbf{U}^{(\ell)}\}$
- 7: **for** $j = 1, \dots, J$ **do**
- 8: $\mathbf{P}_{d,j}^{(\ell,\iota+1)}[k], \mu_{d,j}^*[k] \leftarrow^{\frac{\text{Algorithm 2}}{t_{d,\max}}} \{\mathbf{P}^{(\ell,\iota)}\}, \mathbf{A}^{(\ell,\iota)}, \{\mathbf{U}^{(\ell)}\}$
- 9: $\mathbf{a}^{(\ell,\iota+1)}[k] \leftarrow^{(44c)} \{\mathbf{P}^{(\ell,\iota)}\}, \mathbf{A}^{(\ell,\iota)}, \{\mathbf{U}^{(\ell)}\}, \boldsymbol{\mu}^*$
- 10: $\mathbf{A}^{(\ell,\iota+1)} = \left[\left(\mathbf{a}^{(\ell,\iota+1)}[1] \right)^\top; \dots; \left(\mathbf{a}^{(\ell,\iota+1)}[K] \right)^\top \right]$
- 11: $\iota \leftarrow \iota + 1$
- 12: **until** $\iota > \ell_{\max}$
- 13: $\{\mathbf{P}^{(\ell)}\} \leftarrow \{\mathbf{P}^{(\ell,\iota)}\}$, $\mathbf{A}' \leftarrow \mathbf{A}^{(\ell,\iota)}$
- 14: **return** $\{\mathbf{P}^{(\ell)}\}$, \mathbf{A}'

$$\underset{\mathbf{a}_{m_r}, \forall m_r}{\text{minimize}} \|\mathbf{a}_{m_r} - \mathbf{a}'_{m_r}\|_2^2 \text{ subject to (24f) and (24g)} \quad (46)$$

yields \mathbf{a}'_{m_r} , the m_r th column of \mathbf{A}^* . This is essentially a matrix nearness problem with specified column norms and PARs. It often arises in structured tight frame design problems and is solved via AP [47, 48]. We use the ‘‘nearest vector with low PAR’’ algorithm of [48] to find $\mathbf{a}'_{m_r}^{(\ell)}$ for all m_r recursively at the ℓ th iteration of the BCD-AP MRMC algorithm (see Algorithm 4).

Algorithm 4 Nearest vector method to find $\mathbf{A}^{(\ell)}$

Input: $\mathbf{A}' = [\mathbf{a}'_1, \dots, \mathbf{a}'_{M_r}]$, P_{r,m_r} , γ_{m_r} , $\forall m_r$

Output: $\mathbf{A}^{(\ell)} = [\mathbf{a}_1^{(\ell)}, \dots, \mathbf{a}_{M_r}^{(\ell)}]$

- 1: **for** $m_r = 1, \dots, M_r$ **do**
- 2: Normalize \mathbf{a}'_{m_r} to unit norm; define $\sigma_{m_r} = \sqrt{P_{r,m_r} \gamma_{m_r} / K}$
- 3: $P \leftarrow$ number of elements in \mathbf{a}'_{m_r} with the least magnitude
- 4: $\varpi \leftarrow$ indices of the elements in \mathbf{a}'_{m_r} with the least magnitude
- 5: **if** $\min(|\mathbf{a}'_{m_r}[k]|) = 0, \forall k \in \varpi$ **then**

$$\mathbf{a}_{m_r}^{(\ell)}[k] = \begin{cases} \sqrt{\frac{P_{r,m_r}(K-P)\sigma_{m_r}^2}{P}} & \text{if } k \in \varpi, \\ \sigma_{m_r} e^{j\angle \mathbf{a}'_{m_r}[k]} & \text{if } k \notin \varpi \end{cases}$$
- 6: **if** $\min(|\mathbf{a}'_{m_r}[k]|) \neq 0, \forall k \in \varpi$ **then**

$$\rho = \sqrt{\frac{P_{r,m_r}(K-P)\sigma_{m_r}^2}{\sum_{k \in \varpi} |\mathbf{a}'_{m_r}[k]|^2}}$$
and it results in
$$\mathbf{a}_{m_r}^{(\ell)}[k] = \begin{cases} \rho \mathbf{a}'_{m_r}[k] & \text{if } k \in \varpi, \\ \sigma_{m_r} e^{j\angle \mathbf{a}'_{m_r}[k]} & \text{if } k \notin \varpi \end{cases}$$
- 7: **return** $\mathbf{A}^{(\ell)} = [\mathbf{a}_1^{(\ell)}, \dots, \mathbf{a}_{M_r}^{(\ell)}]$

D. BCD-AP MRMC algorithm

Once $\{\mathbf{P}^{(\ell)}\}$ and $\mathbf{A}^{(\ell)}$ are known, the LRFs of the ℓ th iteration of the BCD-AP MRMC algorithm $\{\mathbf{U}^{(\ell)}\}$ are updated with the WMMSE solution obtained via BCD (Section IV-A). The full BCD-AP MRMC algorithm is summarized in Algorithm 5, where ℓ_{\max} is the maximum number of iterations.

Algorithm 5 BCD-AP MRMC algorithm to find $\{\mathbf{P}^*\}, \mathbf{A}^*, \{\mathbf{U}^*\}$

Input: ℓ_{\max} , ℓ_{\max} , $t_{u,\max}$, $t_{d,\max}$

Output: Optimal UL/DL precoders $\{\mathbf{P}^*\}$, MIMO radar code matrix \mathbf{A}^* , and LRFs $\{\mathbf{U}^*\}$

- 1: Initialize $\{\mathbf{P}^{(0)}\} \triangleq \{\mathbf{P}_{u,i}^{(0)}[k], \mathbf{P}_{d,j}^{(0)}[k], \forall \{i, j, k\}\}$ and $\mathbf{A}^{(0)} = \left[\mathbf{a}^{(0)}[1]; \dots; \mathbf{a}^{(0)}[K] \right]$
- 2: $\{\mathbf{U}^{(0)}\} \leftarrow^{(34),(35),(36)} \{\mathbf{P}^{(0)}\}$ and $\mathbf{A}^{(0)}$
- 3: Set the alternating projection iteration index $\ell = 0$
- 4: **repeat**
- 5: $\{\mathbf{P}^{(\ell+1)}\}, \mathbf{A}' \leftarrow^{\frac{\text{Algorithm 3}}{\ell_{\max}, t_{u,\max}, t_{d,\max}}} \{\mathbf{P}^{(\ell)}\}, \mathbf{A}^{(\ell)}, \{\mathbf{U}^{(\ell)}\}$
- 6: $\mathbf{A}^{(\ell+1)} \leftarrow^{\text{Algorithm 4}} \mathbf{A}'$
- 7: $\{\mathbf{U}^{(\ell+1)}\} \leftarrow^{(34),(35),(36)} \{\mathbf{P}^{(\ell+1)}\}$ and $\mathbf{A}^{(\ell+1)}$
- 8: $\ell \leftarrow \ell + 1$
- 9: **until** $\ell > \ell_{\max}$
- 10: $\{\mathbf{P}^*\} \leftarrow \{\mathbf{P}^{(\ell)}\}$, $\mathbf{A}^* \leftarrow \mathbf{A}^\ell$, and $\{\mathbf{U}^*\} \leftarrow \{\mathbf{U}^{(\ell)}\}$
- 11: **return** $\{\mathbf{P}^*\}, \mathbf{A}^*, \{\mathbf{U}^*\}$

E. Complexity and Convergence

Algorithms 1 and 2 are guaranteed to converge to $\boldsymbol{\lambda}^*$ and $\boldsymbol{\mu}^*$ as long as $\beta_{u,i}^{(t)}[k]$, $\beta_d^{(t)}[k]$, $\varepsilon_{u,i}^{(t)}[k]$, and $\varepsilon_{d,j}^{(t)}[k]$ are sufficiently small; their computational complexities are $\mathcal{O}(I)$ and $\mathcal{O}(J)$, respectively [42]. The WMMSE-MRMC algorithm converges locally because its alternating procedure produces a monotonically non-increasing sequence of iterates, $\{\Xi_{\text{wmmse}}^{(\ell,\iota)}\}$; see Appendix C of [38] for proof. However, Ξ_{wmmse} is not jointly convex on $\{\mathbf{P}^{(\ell)}\}$ and $\mathbf{A}^{(\ell)}$. Hence, the global convergence of the WMMSE-MRMC algorithm is not

guaranteed [31, 38]. The computational complexities of WMMSE-MRMC to update $\mathbf{P}_{u,i}[k]$, $\mathbf{P}_{d,j}[k]$, and $\mathbf{a}[k]$ at each iteration are, respectively, $\mathcal{O}((N_i^u D_i^u)^3)$, $\mathcal{O}((M_c D_j^d)^3)$, and $\mathcal{O}(M_r^3)$, primarily because of complexity in solving Sylvester equations. The objective function in (46) satisfies the Kurdyka-Łojasiewicz property. Therefore, the sequence $\{\mathbf{a}_{m_r}^{(\ell)}\}$ generated by Algorithm 4 at the ℓ^{th} step is convergent for all m_r [47]. The BCD-AP MRMC algorithm also converges to the local optimum with a convergence rate of $\mathcal{O}(1/\ell_{\max})$ [43]. In general, different initialization methods affect the local convergence rate and optimal values of BCD-AP MRMC. As we demonstrate in the next section, one way to approach the global optimum of the WMMSE-RC is through a large number of random initializations [38].

V. NUMERICAL EXPERIMENTS

We validated our spectral co-design approach through extensive numerical experiments. Throughout this section, we set the noise power at J DL UEs, N_r radar Rx and BS Rx to $\sigma_0^2 = 0.01$. Unless otherwise stated, we use the following parameter values: radar and communications Tx and Rx antennas are $M_r = N_r = M_c = N_c = 4$, $I = J = 2$, $N_i^u = d_i^u = 4$, $N_j^d = d_j^d = 3$, $\eta_{m_r,j}^2/\sigma_0^2 = 1$ dB, for all $\{m_r, i, j\}$; number of frames $K = 8$, symbols per frame $N = 8$, CUT index $n = 4$, maximum Tx power for the UL $P_U = 1$ and DL $P_d = 2$; QoS of UL and DL $R_u = R_d = 0.3$ bits/channel use; radar Tx power $P_{r,m_r} = 1$ and PAR levels $\gamma_{m_r} = 2$ for all $\{m_r\}$; channel variances are determined by the channel signal-to-noise-ratios (SNRs) $\text{SNR}_r \triangleq \eta_{m_r, \text{tr}}^2/\sigma_0^2 = 5$ dB, $\text{SNR}_{\text{Btr}} \triangleq \eta_{\text{Bt}, n_r}^2/\sigma_0^2 = 1$ dB, $\text{SNR}_{\text{Bmr}} \triangleq \eta_{\text{Bm}, n_r}^2/\sigma_0^2 = 2$ dB, $\text{SNR}_u \triangleq \eta_{u,i}^2/\sigma_0^2 = 2$ dB, $\text{SNR}_d \triangleq \eta_{d,j}^2/\sigma_0^2 = 2$ dB, $\text{SNR}_{\text{BB}} \triangleq \eta_{\text{BB}}^2/\sigma_0^2 = 1$ dB, $\text{SNR}_{\text{ud}} \triangleq \eta_{i,j}^2/\sigma_0^2 = 1$ dB, $\text{SNR}_{\text{rB}} \triangleq \eta_{m_r, \text{B}}^2/\sigma_0^2 = 2$ dB, $\text{SNR}_{\text{rd}} \triangleq \eta_{m_r, r}^2/\sigma_0^2 = 2$ dB for all $\{m_r, n_r, i, j\}$; the normalized Doppler shifts $f_{m_r, \text{tr}}$ and f_{Btr} are uniformly distributed variables in $[0.05, 0.325]$; the clutter-to-noise-ratio (CNR) at n_r^{th} radar Rx $\text{CNR}_r = \sigma_{c, n_r}^2/\sigma_0^2 = 1$ and $\rho_c = 0.5$ for $\{n_r\}$; maximum iteration numbers for Algorithms 1 and 2 $t_{\max} = 7$, WMMSE-MRMC algorithm $\ell_{\max} = 8$, and BCD-AP MRMC algorithm $\ell_{\max} = 20$. We use uniform weights $\alpha_i^u = \alpha_j^d = \alpha_{n_r}^r = \frac{1}{(I+J+N_r)}$ for all $\{n_r, i, j\}$.

A. Convergence Analysis

We first demonstrate the convergence of BCD-AP MRMC. To approach the optimal solution, we initialize the precoders $\{\mathbf{P}^{(0)}\}$ in two different ways. The ‘initialization 1’ is computationally efficient because we choose singular vectors of $\mathbf{P}_{u,i}^{(0)}[k]$ and $\mathbf{P}_{d,j}^{(0)}[k]$ to be the right singular matrices of $\mathbf{H}_{i,B}$ and $\mathbf{H}_{B,j}$, respectively; and the non-zero entries of the singular values of $\mathbf{P}_{u,i}^{(0)}[k]$ and $\mathbf{P}_{d,j}^{(0)}[k]$ are set to be P_U/D_i^u and P_d/J , respectively, for all $\{i, j, k\}$. The ‘initialization 2’ generates the singular vectors of $\mathbf{P}_{u,i}^{(0)}[k]$ and $\mathbf{P}_{d,j}^{(0)}[k]$ as two random matrices drawn from $\mathcal{CN}(0, 1)$ and singular values in the same way as the ‘initialization 1’. Figure 3 shows the convergence of BCD-AP MRMC in terms of $I_{\text{CWSM}}^{(\ell)}$ with respect to iteration index ℓ for different SNR_r values. The BCD-AP MRMC converges under all these different initialization conditions and SNR levels. The discrepancy between the two initialization methods is small with respect to I_{CWSM} and I_r , but large with I_{fd} .

B. Radar Detection Performance

We investigated the detection performance of the statistical MIMO radar using the designed code matrix \mathbf{A} . Consider the binary hypothesis testing formulation for target detection as

$$\begin{cases} \mathcal{H}_0 : \mathbf{y}_r = \mathbf{y}_{\text{cr}} + \mathbf{y}_{\text{Bmr}} + \mathbf{y}_{\text{Ur}} + \mathbf{z}_r \\ \mathcal{H}_1 : \mathbf{y}_r = \mathbf{y}_{\text{tr}} + \mathbf{y}_{\text{cr}} + \mathbf{y}_{\text{Bmr}} + \mathbf{y}_{\text{Ur}} + \mathbf{z}_r \end{cases} \quad (47)$$

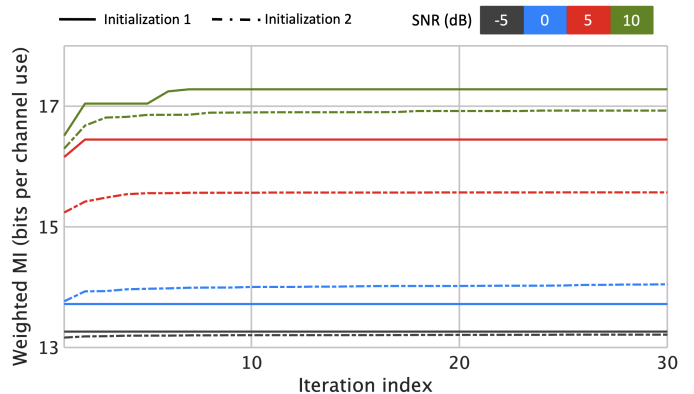


Fig. 3. Convergence behaviors of the BCD-AP MRMC algorithm with two initialization methods and multiple SNR_r values.

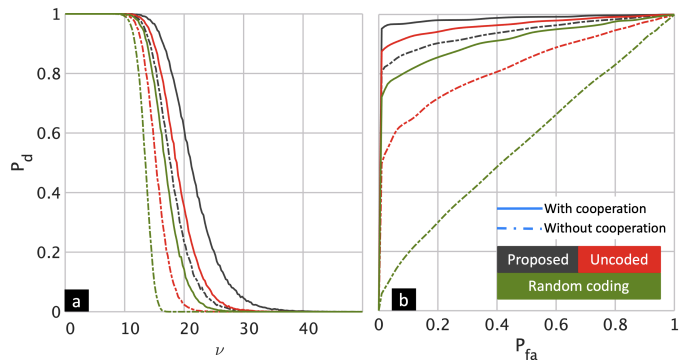


Fig. 4. Target detection performance of the coexisting system compared with other radar codes and cooperation schemes using the NP detector. (a) P_d versus ν (b) ROC of the NP detector.

where $\mathbf{y}_r = [\mathbf{y}_{r,1}^\top; \dots; \mathbf{y}_{r,N_r}^\top]^\top$ and $\mathbf{y}_{\text{tr}} = [\mathbf{y}_{\text{tr},1}^\top; \dots; \mathbf{y}_{\text{tr},N_r}^\top]^\top$. Denote $\mathbf{y}_{\text{in}}^r \triangleq \mathbf{y}_{\text{cr}} + \mathbf{y}_{\text{Bmr}} + \mathbf{y}_{\text{Ur}} + \mathbf{z}_r = \left[(\mathbf{y}_{\text{in},n_r}^r)^\top; \dots; (\mathbf{y}_{\text{in},N_r}^r)^\top \right]^\top$ and its CM $\mathbf{R}_{\text{in}} = \bigoplus_{n_r=1}^{N_r} \mathbf{R}_{\text{in},n_r}$. Similarly, define $\bar{\mathbf{y}}_{r,n_r} = \mathbf{R}_{\text{in},n_r}^{-1/2} \mathbf{y}_{r,n_r}$ and its CM $\mathbf{G}_{n_r} = \mathbf{R}_{\text{in},n_r}^{-1/2} \mathbf{R}_{u,n_r} \mathbf{R}_{\text{in},n_r}^{-1/2}$. Rewrite hypothesis testing problem as

$$\begin{cases} \mathcal{H}_0 : \bar{\mathbf{y}}_r \sim \mathcal{CN}(\mathbf{0}, \mathbf{I}) \\ \mathcal{H}_1 : \bar{\mathbf{y}}_r \sim \mathcal{CN}(\mathbf{0}, \mathbf{I} + \mathbf{G}) \end{cases} \quad (48)$$

where the block diagonal matrix $\mathbf{G} = \bigoplus_{n_r=1}^{N_r} \mathbf{G}_{n_r}$. The eigendecomposition of \mathbf{G}_{n_r} is $\mathbf{G}_{n_r} = \mathbf{V}_{n_r} \mathbf{\Lambda}_{n_r} \mathbf{V}_{n_r}^\dagger$, where the columns of \mathbf{V}_{n_r} and the diagonal entries of $\mathbf{\Lambda}_{n_r} \triangleq \text{diag}[\delta_{1,n_r}, \dots, \delta_{K,n_r}]$ are, respectively, the eigenvectors and eigenvalues of \mathbf{G}_{n_r} , the k^{th} eigenvalue being δ_{k,n_r} . Using the Woodbury matrix identity and the eigendecomposition of \mathbf{G}_{n_r} , the test statistic is

$$\begin{aligned} T(\bar{\mathbf{y}}) &= \sum_{n_r=1}^{N_r} T(\bar{\mathbf{y}}_{r,n_r}) = \sum_{n_r=1}^{N_r} \bar{\mathbf{y}}_{r,n_r}^\dagger (\mathbf{I} - (\mathbf{G}_{n_r} + \mathbf{I})^{-1}) \bar{\mathbf{y}}_{r,n_r} \\ &= \sum_{n_r=1}^{N_r} \bar{\mathbf{y}}_{r,n_r}^\dagger \mathbf{V}_{n_r} (\mathbf{\Lambda}^{-1} + \mathbf{I})^{-1} \mathbf{V}_{n_r}^\dagger \bar{\mathbf{y}}_{r,n_r} \end{aligned} \quad (49)$$

Denote $\hat{\mathbf{y}}_{r,n_r} = \mathbf{V}_{n_r}^\dagger \bar{\mathbf{y}}_{r,n_r} = [\hat{y}_{n_r}[1], \dots, \hat{y}_{n_r}[K]]$. Then, the Neyman-Pearson (NP) detector is [51]

$$T(\bar{\mathbf{y}}) = \sum_{n_r=1}^{N_r} \sum_{k=1}^K \frac{\delta_{k,n_r} |\hat{y}_{n_r}[k]|^2}{1 + \delta_{k,n_r}} \underset{\mathcal{H}_2}{\overset{\mathcal{H}_1}{\geq}} \nu, \quad (50)$$

where ν is the threshold selected to guarantee a certain detection performance. We performed Monte Carlo (MC) simulations to evaluate the probability of detection P_d and the Rx operating characteristic (ROC) (curve of P_d versus probability of false alarm P_{fa}) of the NP detector. Figures 4a and 4b show P_d with respect to ν and ROC,

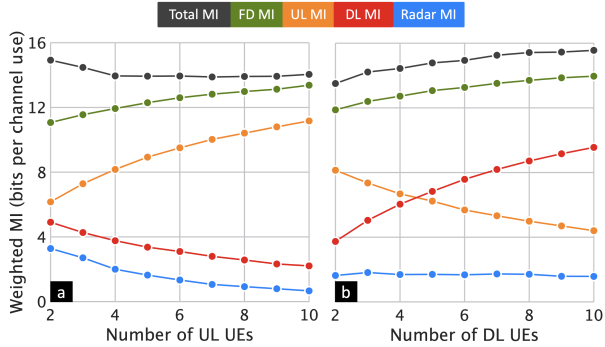


Fig. 5. Performance of the coexisting system evaluation compared with increasing numbers of (a) UL and (b) DL UEs.

respectively, for various waveforms and cooperation modes. Here, presence or absence of cooperation indicates whether or not the DL signals $\mathbf{y}_{\text{Bt},n_r}$ are incorporated in $\mathbf{y}_{\text{t},n_r}$ for all n_r . For the m_r th radar Tx, the uncoded waveform is $\mathbf{a}_{m_r} = \sqrt{\frac{P_{r,m_r}}{K}} \mathbf{1}_K$ and randomly coded waveform is $\mathbf{a}_{m_r} = \sqrt{\frac{P_{r,m_r}}{K}} \mathbf{u}_{m_r}$, where $\{\mathbf{u}_{m_r}\}$ is a unitary basis. We generated 5000 realizations of $\bar{\mathbf{y}}_r$ under hypothesis \mathcal{H}_1 to estimate P_d and \mathcal{H}_0 to estimate P_{fa} based on ν for each mode. Figures 4a and 4b illustrate that our optimized radar waveform outperforms the all-ones (uncoded) and random coding schemes, and that the cooperation between the radar and BS boosts the radar detection performance. For example, in Fig. 4b, with $P_{\text{fa}} = 0.1$, when radar codes and UL/DL precoders obtained via Algorithm 5 are used along with radar-DL cooperation, this yields approximately 8% improvement in P_d over the non-cooperation mode, 6% over the all-ones waveform with cooperation, and 13% over random code with cooperation. We observe that even without the cooperation, our algorithm enables the MIMO radar to provide a competitive detection performance.

C. FD Communications Performance

We explored the effect on the system performance with increasing UEs. Figures 5a and 5b depict weighted UL MI $I_U \triangleq \sum_k \sum_i \alpha_i^u I_{u,i}[k]$, weighted DL MI $I_D \triangleq \sum_k \sum_j \alpha_j^d I_{d,j}[k]$, radar MI $I_R \triangleq \alpha_{n_r}^r \sum_{n_r} I_{r,n_r}[k]$, total weighted FD MI and I_{CWSM} as the number of UL UEs and DL UEs are varied, respectively. The power levels are set at $P_u = I$ and $P_d = J$. As the number of UL UEs increases from $I = 2$ to $I = 10$ with the number of DL UEs fixed at $J = 2$, the performances of DL UEs and radar RxS deteriorate owing to the increasing UL interference. On the other hand, the performance of the UL drops while that of the MIMO radar remains relatively stable as the number of DL UEs rises from $J = 2$ to $J = 10$ with $I = 2$. We observe that the total system performance measure I_{CWSM} is enhanced with a higher DL power because of the radar-DL cooperation whereas I_{CWSM} declines with a rising UL power.

D. Joint Radar-Communications Performance

Finally, we evaluated the co-design performance by observing the mutual impact of the statistical MIMO radar and IBFD MU-MIMO communications on each other. Figure 6 compares the CWSMs achieved by the IBFD MU-MIMO as well as the HD MU-MIMO communications jointly operating with a statistical MIMO radar. We also included the cooperation and non-cooperation modes for IBFD MU-MIMO and DL MU-MIMO communications. In practice, the radar-enabled interference channel gains, namely $\eta_{r,j}^2$ and η_{rB}^2 are fractions of the radar-target channel gains η_{m_r,n_r}^2 . As a result, the severity of the radar-enabled interference with the communications systems are also related to the radar-target channel gains. Specifically, we set $\text{SNR}_r = 0.8\text{SNR}_{rB}$ and $\text{SNR}_r = 0.6\text{SNR}_{rd}$. We observed that when the radar power dominates the co-designed system, the impact

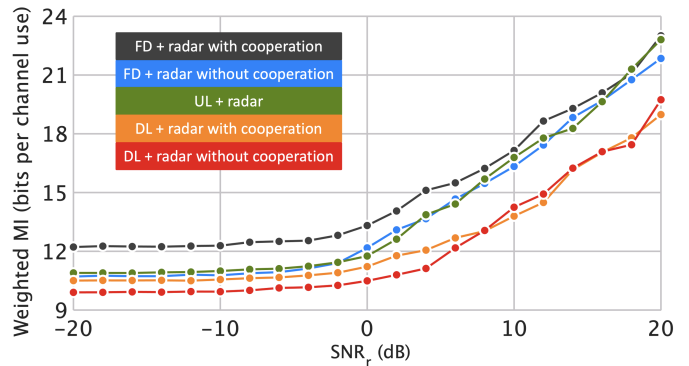


Fig. 6. Evaluation of the MU-MIMO communications with different transmission schemes under various radar SNRs

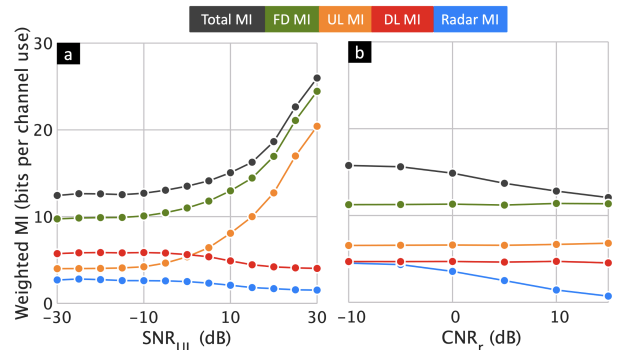


Fig. 7. Joint radar and communications interference analysis. (a) System performance vs UL SNRs (b) System performance vs CNR.

of radar-DL cooperation is less apparent. In Fig. 7, the performance of co-designed system is shown to vary with different UL SNR and CNR values. Here, $\text{SNR}_{ur} = 0.7\text{SNR}_u$ and $\text{SNR}_{ud} = 0.8\text{SNR}_u$ for Fig. 7a and $\text{SNR}_{rB} = 0.5\text{CNR}_r$ and $\text{SNR}_{rd} = 0.5\text{CNR}_r$ for Fig. 7b. Note that the DL and radar weighted MIs decline by approximately 30% and 45%, respectively, when the UL-DL and UL-radar interfering signal powers are 10^6 times higher. This demonstrates that the designed precoders and radar codes sustain the DL and radar performances despite a high UL Tx power. Meanwhile, from Fig. 7b, the clutter affects the MIMO radar more than the FD communications UEs because the proposed method mitigates the power projected to the interfering channels \mathbf{H}_{rB} and $\mathbf{H}_{r,j}$ from $\{\mathbf{a}[k]\}$.

VI. SUMMARY

In this work, we proposed a spectral co-design for a statistical MIMO radar and an IBFD MU-MIMO communications system. Prior works either largely consider co-located MIMO radars, focus on coexistence solutions, or partially analyze MIMO communications. We take a wholesome view of the problem by jointly designing several essential aspects of such a co-design: UL/DL precoders, MIMO radar code matrix, and LRFs for both systems. Our proposed BCD-AP MRMC algorithm not only guarantees convergence but also provides performance benefits for both systems. The radar codes generated by BCD-AP MRMC significantly increase the probability of detection over conventional waveforms. We also showed that the cooperation between radar and DL signals is beneficial for target detection. The co-designed DL and radar are resilient to considerable UL interference. Similarly, using our optimized precoders and radar codes, the DL and UL rates remain stable as the CNR is increased.

APPENDIX A
PROOF OF THEOREM 2

Solving (42) yields the lower bounds of (40). The difference between the lower bound and the actual optimal value is the optimal duality gap. To equivalently obtain $\{\mathbf{P}^*\}$ and \mathbf{A}' with (42), strong duality ought to hold for the primal problem (33), i.e., the optimal duality gap needs to be zero. However, the QoS constraints (37b) – (37c) are non-concave leading to a non-zero duality gap. To bypass this problem, we apply the Taylor series to obtain linear approximations of $R_{u,i}[k]$ and $R_{d,j}[k]$. The first-order Taylor series expansion of a real-valued function with complex-valued matrix arguments $f(\mathbf{X}, \mathbf{X}^*) : \mathbb{C}^{N \times Q} \times \mathbb{C}^{N \times Q} \rightarrow \mathbb{R}$ around \mathbf{X}_0 produces [52]

$$f(\mathbf{X}, \mathbf{X}^*) = f(\mathbf{X}_0, \mathbf{X}_0^*) + \text{vec}^\top \left(\frac{\partial}{\partial \mathbf{X}_0} f(\mathbf{X}_0, \mathbf{X}_0^*) \right) \text{vec}(\mathbf{X} - \mathbf{X}_0) + \text{vec}^\top \left(\frac{\partial}{\partial \mathbf{X}_0^*} f(\mathbf{X}_0, \mathbf{X}_0^*) \right) \text{vec}(\mathbf{X}^* - \mathbf{X}_0^*). \quad (51)$$

Assume $\tilde{\mathbf{P}}_{u,i}[k]$ is the estimate of $\mathbf{P}_{u,i}[k]$ from the previous iteration. A similar Taylor series expansion of $R_{u,i}[k]$ at $\tilde{\mathbf{P}}_{u,i}[k]$ gives

$$R_{u,q}[k](\mathbf{P}_{u,i}[k]) \approx R_{u,q}[k](\tilde{\mathbf{P}}_{u,i}[k]) + \text{vec} \left\{ \frac{\partial \left(R_{u,q}[k](\tilde{\mathbf{P}}_{u,i}[k]) \right)}{\partial \tilde{\mathbf{P}}_{u,i}[k]} \right\}^\top \text{vec} \left\{ \mathbf{P}_{u,i}[k] - \tilde{\mathbf{P}}_{u,i}[k] \right\} + \text{vec} \left\{ \frac{\partial \left(R_{u,q}[k](\tilde{\mathbf{P}}_{u,i}^*[k]) \right)}{\partial \tilde{\mathbf{P}}_{u,i}^*[k]} \right\}^\top \text{vec} \left\{ \mathbf{P}_{u,i}^*[k] - \tilde{\mathbf{P}}_{u,i}^*[k] \right\}. \quad (52)$$

Likewise, we find the linear approximations of $R_{u,q}[k](\mathbf{P}_{d,j}[k])$, $R_{u,q}[k](\mathbf{a}[k])$, $R_{d,j}[k](\mathbf{P}_{u,i}[k])$, $R_{d,j}[k](\mathbf{P}_{d,j}[k])$, and $R_{d,j}[k](\mathbf{a}[k])$. Note that Ξ_{wmmse} is multi-concave, namely Ξ_{wmmse} is not jointly convex in $\mathbf{P}_{u,i}[k]$, $\mathbf{P}_{d,j}[k]$, and $\mathbf{a}[k]$ but convex in each individual variable provided the rest of the variables are fixed [31, 43]. As a result, we have a fully convex version of (40) and thus the optimal duality gap between (40) and (42) is reduced to zero [42]. Hence, $\{\mathbf{P}^*\}$ and $\mathbf{A}' = [(\mathbf{a}'[1])^\top, \dots, (\mathbf{a}'[K])^\top]^\top$ in (40) are obtained by solving (42). This concludes the proof.

APPENDIX B
DERIVATION OF GRADIENTS

Adopting the notations from [52] and [49], we denote the complex gradient operator for a scalar real-valued function with a complex-valued matrix argument $f(\mathbf{Z}, \mathbf{Z}^*)$ as $\nabla_{\mathbf{Z}} f = \frac{\partial f}{\partial \mathbf{Z}^*}$. From the derivative formula $\frac{\partial}{\partial \mathbf{X}^*} \text{Tr}(\mathbf{B}^\top \mathbf{X} \mathbf{C} \mathbf{X} \mathbf{B}) = \mathbf{C}^\top \mathbf{X} \mathbf{B} \mathbf{B}^\top + \mathbf{C} \mathbf{X} \mathbf{B} \mathbf{B}^\top$ [49], the gradients of Ξ_{UL} and Ξ_{DL} with respect to $\mathbf{P}_{u,i}[k]$, $\mathbf{P}_{d,j}[k]$ and $\mathbf{a}[k]$, respectively, are

$$\nabla_{\mathbf{P}_{u,i}[k]} \Xi_{\text{UL}} = \mathbf{H}_{i,B}^\dagger \boldsymbol{\xi}_{\text{UL}} \mathbf{H}_{i,B} \mathbf{P}_{u,i}[k], \quad (53a)$$

$$\nabla_{\mathbf{P}_{d,j}[k]} \Xi_{\text{UL}} = \mathbf{H}_{\text{BB}}^\dagger \boldsymbol{\xi}_{\text{UL}} \mathbf{H}_{\text{BB}} \mathbf{P}_{d,j}[k], \quad (53b)$$

$$\nabla_{\mathbf{a}[k]} \Xi_{\text{UL}} = \mathbf{H}_{\text{rB}}^\dagger \boldsymbol{\xi}_{\text{UL}} \mathbf{H}_{\text{rB}} \mathbf{a}[k], \quad (53c)$$

$$\nabla_{\mathbf{P}_{u,i}[k]} \Xi_{\text{DL}} = \sum_{g=1}^J \mathbf{H}_{i,g}^\dagger \boldsymbol{\xi}_{d,g} \mathbf{H}_{i,g} \mathbf{P}_{u,i}[k], \quad (53d)$$

$$\nabla_{\mathbf{P}_{d,j}[k]} \Xi_{\text{DL}} = \sum_{g=1}^J \mathbf{H}_{B,g}^\dagger \boldsymbol{\xi}_{d,g} \mathbf{H}_{B,g} \mathbf{P}_{d,j}[k] \quad (53e)$$

$$\text{and } \nabla_{\mathbf{a}[k]} \Xi_{\text{DL}} = \sum_{g=1}^J \mathbf{H}_{r,g}^\dagger \boldsymbol{\xi}_{d,g} \mathbf{H}_{r,g} \mathbf{a}[k], \quad (53f)$$

where $\boldsymbol{\xi}_{\text{UL}}[k] = \sum_{q=1}^I \alpha_q^u \mathbf{U}_{u,q}^\dagger[k] \mathbf{W}_{u,q}[k] \mathbf{U}_{u,q}[k]$ and $\boldsymbol{\xi}_{d,g}[k] = \alpha_g^d \mathbf{U}_{d,g}^\dagger[k] \mathbf{W}_{d,g}[k] \mathbf{U}_{d,g}[k]$. The gradients of Ξ_r with respect to $\mathbf{P}_{u,i}[k]$, $\mathbf{P}_{d,j}[k]$, and $\mathbf{a}[k]$, respectively, are

$$\begin{aligned} \nabla_{\mathbf{P}_{u,i}[k]} \Xi_r &= \sum_{n_r=1}^{N_r} \eta_{i,n_r}^2 \sum_{m=1}^K \mathbf{P}_{u,i}[m] \mathbf{d}_{u,i}[m] \xi_{n_r}(m, k) \mathbf{d}_{u,i}^\dagger[k], \\ &= \sum_{n_r=1}^{N_r} \eta_{i,n_r}^2 \sum_{m \neq k}^K \mathbf{P}_{u,i}[m] \mathbf{d}_{u,i}[m] \xi_{n_r}(m, k) \mathbf{d}_{u,i}^\dagger[k] \\ &\quad + \sum_{n_r=1}^{N_r} \eta_{i,n_r}^2 \mathbf{P}_{u,i}[k] \mathbf{d}_{u,i}[k] \xi_{n_r}(k, k) \mathbf{d}_{u,i}^\dagger[k] \end{aligned}$$

$$\begin{aligned} \nabla_{\mathbf{P}_{d,j}[k]} \Xi_r &= \sum_{n_r=1}^{N_r} \mathbf{J}_B^\top \boldsymbol{\Sigma}_{t,n_r} \sum_{m=1}^K \mathbf{s}_{t,n_r}[m] \xi_{n_r}(m, k) \mathbf{d}_{d,j}^\dagger[k] + \\ &\quad \sum_{n_r=1}^{N_r} \eta_{\text{Bm},n_r}^2 \sum_{m=1}^K \sum_{g=1}^J \mathbf{P}_{d,g}[m] \mathbf{d}_{d,g}[m] \xi_{n_r}(m, k) \mathbf{d}_{d,j}^\dagger[k], \end{aligned}$$

$$\begin{aligned} \nabla_{\mathbf{a}[k]} \Xi_r &= \sum_{n_r=1}^{N_r} \mathbf{Q}_{r,n_r}^\dagger \mathbf{J}_r^\top \boldsymbol{\Sigma}_{t,n_r} \sum_{m=1}^K \mathbf{s}_{t,n_r}[m] \xi_{n_r}(m, k) \\ &= \sum_{n_r=1}^{N_r} \mathbf{Q}_{r,n_r}^\dagger \mathbf{J}_r^\top \boldsymbol{\Sigma}_{t,n_r} \sum_{m \neq k}^K \mathbf{s}_{t,n_r}[m] \xi_{n_r}(m, k) \\ &\quad + \sum_{n_r=1}^{N_r} \mathbf{a}[k] \eta_{n,n_r}^2 \xi_{n_r}(k, k), \end{aligned}$$

where $\xi_{n_r}(m, k) = \mathbf{u}_{r,n_r}^\top[m] \mathbf{W}_{r,n_r}^\top \mathbf{u}_{r,n_r}^*[k]$. The derivatives of f in (51) with respect to \mathbf{X}^* are thus approximated as $\frac{\partial f}{\partial \mathbf{X}^*} = \frac{\partial}{\partial \mathbf{X}_0^*} f(\mathbf{X}_0, \mathbf{X}_0^*)$. The chain rule for a scalar function $g(\mathbf{U}(\mathbf{X}, \mathbf{X}^*), \mathbf{U}^*(\mathbf{X}, \mathbf{X}^*))$ where g is dependent on \mathbf{X}^* through the matrix \mathbf{U} is [49]

$$\frac{\partial g}{\partial \mathbf{X}^*} = \frac{\text{Tr} \left\{ \left(\frac{\partial g}{\partial \mathbf{U}} \right)^\top \partial \mathbf{U} \right\}}{\partial \mathbf{X}^*} + \frac{\text{Tr} \left\{ \left(\frac{\partial g}{\partial \mathbf{U}^*} \right)^\top \partial \mathbf{U}^* \right\}}{\partial \mathbf{X}^*}. \quad (54)$$

From (54), the derivative of the logarithm of determinant formula $\partial \log |\mathbf{X}| = \text{Tr} \{ \mathbf{X}^{-1} \partial \mathbf{X} \}$ [49, 52]. Further, the derivatives of $R_{u,q}[k]$ and $R_{d,j}[k]$ with respect to $\mathbf{P}_{u,i}[k]$, $\mathbf{P}_{d,j}[k]$, and $\mathbf{a}[k]$ based on their Taylor series expansions in the initial approximations $\tilde{\mathbf{P}}_{u,i}[k]$, $\tilde{\mathbf{P}}_{d,j}[k]$, and $\tilde{\mathbf{a}}[k]$, respectively, are

$$\begin{aligned} \nabla_{\mathbf{P}_{u,i}[k]} R_{u,q}[k] &= \mathbf{H}_{i,B}^\dagger \boldsymbol{\Psi}_{u,i} \tilde{\mathbf{P}}_{u,i}[k] \boldsymbol{\Upsilon}_{u,i}^{-1}, \quad q = i, \\ \nabla_{\mathbf{P}_{u,i}[k]} R_{u,q}[k] &= -\mathbf{H}_{i,B}^\dagger \boldsymbol{\Psi}_{u,q} \mathbf{P}_{u,q}[k] \boldsymbol{\Upsilon}_{u,q}^{-1} \\ &\quad \mathbf{P}_{u,q}[k] \boldsymbol{\Psi}_{u,q}^\dagger \mathbf{H}_{i,B} \tilde{\mathbf{P}}_{u,i}[k], \quad q \neq i, \\ \nabla_{\mathbf{P}_{d,j}[k]} R_{u,q}[k] &= -\mathbf{H}_{\text{BB}}^\dagger \boldsymbol{\Psi}_{u,q} \mathbf{P}_{u,q}[k] \boldsymbol{\Upsilon}_{u,q}^{-1} \mathbf{P}_{d,j}^\dagger[k] \boldsymbol{\Psi}_{u,q}^\dagger \mathbf{H}_{\text{BB}} \mathbf{P}_{d,j}[k], \\ \nabla_{\mathbf{a}[k]} R_{u,q}[k] &= -\mathbf{H}_{\text{rB}}^\dagger \boldsymbol{\Psi}_{u,q} \mathbf{P}_{u,q}[k] \boldsymbol{\Upsilon}_{u,q}^{-1} \mathbf{P}_{d,j}^\dagger[k] \boldsymbol{\Psi}_{u,q}^\dagger \mathbf{H}_{\text{rB}} \mathbf{a}[k], \\ \nabla_{\mathbf{P}_{u,i}[k]} R_{d,j}[k] &= -\mathbf{H}_{i,g}^\dagger \boldsymbol{\Psi}_{d,g} \mathbf{P}_{d,g}[k] \boldsymbol{\Upsilon}_{d,g}^{-1} \mathbf{P}_{d,g}^\dagger[k] \boldsymbol{\Psi}_{d,g}^\dagger \mathbf{H}_{i,g} \tilde{\mathbf{P}}_{u,i}[k], \\ \nabla_{\mathbf{P}_{d,j}[k]} R_{d,j}[k] &= \mathbf{H}_{B,j}^\dagger \boldsymbol{\Psi}_{d,j} \tilde{\mathbf{P}}_{d,j}[k] \boldsymbol{\Upsilon}_{d,j}^{-1}, \quad g = j, \\ \nabla_{\mathbf{P}_{d,j}[k]} R_{d,j}[k] &= -\mathbf{H}_{B,j}^\dagger \boldsymbol{\Psi}_{d,g} \mathbf{P}_{d,g}[k] \boldsymbol{\Upsilon}_{d,g}^{-1} \\ &\quad \mathbf{P}_{d,g}^\dagger[k] \boldsymbol{\Psi}_{d,g}^\dagger \mathbf{H}_{B,j} \tilde{\mathbf{P}}_{d,j}[k], \quad g \neq j, \\ \nabla_{\mathbf{a}[k]} R_{d,j}[k] &= -\mathbf{H}_{r,g}^\dagger \boldsymbol{\Psi}_{d,g} \mathbf{P}_{d,g}[k] \boldsymbol{\Upsilon}_{d,g}^{-1} \mathbf{P}_{d,g}^\dagger[k] \boldsymbol{\Psi}_{d,g}^\dagger \mathbf{H}_{r,g} \mathbf{a}[k], \quad (55) \end{aligned}$$

where $\boldsymbol{\Upsilon}_{u,i}[k] = \mathbf{I} + \tilde{\mathbf{P}}_{u,i}^\dagger[k] \mathbf{H}_{i,B}^\dagger (\mathbf{R}_{\text{in},i}^u[k])^{-1} \mathbf{H}_{i,B} \tilde{\mathbf{P}}_{u,i}[k]$
 $\boldsymbol{\Upsilon}_{u,q} = \mathbf{I} + \mathbf{P}_{u,q}^\dagger[k] \mathbf{H}_{q,B}^\dagger (\mathbf{R}_{\text{in},q}^u[k])^{-1} \mathbf{H}_{q,B} \mathbf{P}_{u,q}[k]$, $q \neq i$
 $\boldsymbol{\Upsilon}_{d,g} = \mathbf{I} + \tilde{\mathbf{P}}_{d,j}^\dagger[k] \mathbf{H}_{B,j}^\dagger (\mathbf{R}_{\text{in},j}^d[k, l])^{-1} \mathbf{H}_{B,j} \tilde{\mathbf{P}}_{d,j}[k]$,
 $\boldsymbol{\Upsilon}_{d,g} = \mathbf{I} + \mathbf{P}_{d,g}^\dagger[k] \mathbf{H}_{B,g}^\dagger (\mathbf{R}_{\text{in},g}^d[k])^{-1} \mathbf{H}_{B,g} \mathbf{P}_{d,g}[k]$, $g \neq j$,
 $\boldsymbol{\Psi}_{u,q} = (\mathbf{R}_{\text{in},q}^u[k])^{-1}$ and $\boldsymbol{\Psi}_{d,g} = (\mathbf{R}_{\text{in},g}^d[k])^{-1} \mathbf{H}_{B,g}$.

REFERENCES

- [1] K. V. Mishra, M. R. Bhavani Shankar, V. Koivunen, B. Ottersten, and S. A. Vorobyov, "Toward millimeter wave joint radar communications: A signal processing perspective," *IEEE Signal Process. Mag.*, vol. 36, no. 5, pp. 100–114, 2019.

- [2] S. H. Dokhanchi, B. S. Mysore, K. V. Mishra, and B. Ottersten, "A mmWave automotive joint radar-communications system," *IEEE Trans. Aerosp. Electron. Syst.*, vol. 55, no. 3, pp. 1241–1260, 2019.
- [3] S. Biswas, K. Singh, O. Taghizadeh, and T. Ratnarajah, "Coexistence of MIMO radar and FD MIMO cellular systems with QoS considerations," *IEEE Trans. Wireless Commun.*, vol. 17, no. 11, pp. 7281–7294, 2018.
- [4] C. D'Andrea, S. Buzzi, and M. Lops, "Communications and radar coexistence in the massive MIMO regime: Uplink analysis," *IEEE Trans. Wireless Commun.*, vol. 19, no. 1, pp. 19–33, 2020.
- [5] F. Liu, C. Masouros, A. Li, H. Sun, and L. Hanzo, "MU-MIMO communications with MIMO radar: From co-existence to joint transmission," *IEEE Trans. Wireless Commun.*, vol. 17, no. 4, pp. 2755–2770, 2018.
- [6] G. Duggal, S. Vishwakarma, K. V. Mishra, and S. S. Ram, "Doppler-resilient 802.11ad-based ultra-short range automotive joint radar-communications system," *IEEE Trans. Aerosp. Electron. Syst.*, vol. early access, 2020.
- [7] M. Alae-Kerahroodi, K. V. Mishra, M. R. Bhavani Shankar, and B. Ottersten, "Discrete phase sequence design for coexistence of MIMO radar and MIMO communications," in *IEEE Int. Workshop Signal Process. Advances Wireless Commun.*, 2019, pp. 1–5.
- [8] D. Bao, G. Qin, J. Cai, and G. Liu, "A precoding OFDM MIMO radar coexistence with a communication system," *IEEE Trans. Aerosp. Electron. Syst.*, vol. 55, no. 4, pp. 1864–1877, 2019.
- [9] Z. Slavik and K. V. Mishra, "Cognitive interference mitigation in automotive radars," in *IEEE Radar Conf.*, 2019, pp. 1–6.
- [10] A. Ayyar and K. V. Mishra, "Robust communications-centric coexistence for turbo-coded OFDM with non-traditional radar interference models," in *IEEE Radar Conf.*, 2019, pp. 1–6.
- [11] J. A. Mahal, A. Khawar, A. Abdelhadi, and T. C. Clancy, "Spectral coexistence of MIMO radar and MIMO cellular system," *IEEE Trans. Aerosp. Electron. Syst.*, vol. 53, no. 2, pp. 655–668, 2017.
- [12] B. Li and A. Petropulu, "Joint transmit designs for co-existence of MIMO wireless communications and sparse sensing radars in clutter," *IEEE Trans. Aerosp. Electron. Syst.*, vol. 53, no. 6, pp. 2846–2864, 2017.
- [13] J. Qian, M. Lops, L. Zheng, X. Wang, and Z. He, "Joint system design for coexistence of MIMO radar and MIMO communication," *IEEE Trans. Signal Process.*, vol. 66, no. 13, pp. 3504–3519, 2018.
- [14] M. Rihan and L. Huang, "Optimum co-design of spectrum sharing between MIMO radar and MIMO communication systems: An interference alignment approach," *IEEE Trans. Veh. Technol.*, vol. 67, no. 12, pp. 11 667–11 680, 2018.
- [15] E. Grossi, M. Lops, and L. Venturino, "Joint design of surveillance radar and MIMO communication in cluttered environments," *IEEE Trans. Signal Process.*, vol. 68, pp. 1544–1557, 2020.
- [16] Q. He, Z. Wang, J. Hu, and R. S. Blum, "Performance gains from cooperative MIMO radar and MIMO communication systems," *IEEE Signal Process. Lett.*, vol. 26, no. 1, pp. 194–198, 2019.
- [17] S. H. Dokhanchi, M. R. Bhavani Shankar, K. V. Mishra, and B. Ottersten, "Multi-constraint spectral co-design for colocated MIMO radar and MIMO communications," in *IEEE Int. Conf. Acoust. Speech Signal Process.*, 2020, pp. 4567–4571.
- [18] F. Liu, C. Masouros, A. Li, T. Ratnarajah, and J. Zhou, "MIMO radar and cellular coexistence: A power-efficient approach enabled by interference exploitation," *IEEE Trans. Signal Process.*, vol. 66, no. 14, pp. 3681–3695, 2018.
- [19] M. Alae-Kerahroodi, M. R. Bhavani Shankar, K. V. Mishra, and B. Ottersten, "Information theoretic approach for waveform design in coexisting MIMO radar and MIMO communications," in *IEEE Int. Conf. Acoust. Speech Signal Process.*, 2020, pp. 1–5.
- [20] D. Tse and P. Viswanath, *Fundamentals of wireless communication*. Cambridge Univ. Press, 2005.
- [21] A. M. Haimovich, R. S. Blum, and L. J. Cimini, "MIMO radar with widely separated antennas," *IEEE Signal Process. Mag.*, vol. 25, no. 1, pp. 116–129, 2008.
- [22] T. L. Marzetta, "Noncooperative cellular wireless with unlimited numbers of base station antennas," *IEEE Transactions on Wireless Communications*, vol. 9, no. 11, pp. 3590–3600, 2010.
- [23] E. Fishler, A. Haimovich, R. S. Blum, L. J. Cimini, D. Chizhik, and R. A. Valenzuela, "Spatial diversity in radars models and detection performance," *IEEE Trans. Signal Process.*, vol. 54, no. 3, pp. 823–838, 2006.
- [24] K. V. Mishra, Y. C. Eldar, E. Shoshan, M. Namer, and M. Meltin, "A cognitive sub-Nyquist MIMO radar prototype," *IEEE Trans. Aerosp. Electron. Syst.*, vol. 56, no. 2, pp. 937–955, 2020.
- [25] P. Wang, H. Li, and B. Himed, "Moving target detection using distributed MIMO radar in clutter with nonhomogeneous power," *IEEE Trans. Signal Process.*, vol. 59, no. 10, pp. 4809–4820, 2011.
- [26] S. Sun, K. V. Mishra, and A. P. Petropulu, "Target estimation by exploiting low rank structure in widely separated MIMO radar," in *IEEE Radar Conf.*, 2019, pp. 1–6.
- [27] X. Song, P. Willett, S. Zhou, and P. B. Luh, "The MIMO radar and jammer games," *IEEE Trans. Signal Process.*, vol. 60, no. 2, pp. 687–699, 2012.
- [28] M. M. Naghsh, M. Modarres-Hashemi, M. A. Kerahroodi, and E. H. M. Alian, "An information theoretic approach to robust constrained code design for MIMO radars," *IEEE Trans. Signal Process.*, vol. 65, no. 14, pp. 3647–3661, 2017.
- [29] A. Khawar, A. Abdelhadi, and C. Clancy, "Target detection performance of spectrum sharing MIMO radars," *IEEE Sensors J.*, vol. 15, no. 9, pp. 4928–4940, 2015.
- [30] E. Grossi, M. Lops, and L. Venturino, "Joint design of surveillance radar and MIMO communication in cluttered environments," *IEEE Trans. Signal Process.*, vol. 68, pp. 1544–1557, 2020.
- [31] P. Aquilina, A. C. Cirik, and T. Ratnarajah, "Weighted sum rate maximization in full-duplex multi-user multi-cell MIMO networks," *IEEE Trans. Commun.*, vol. 65, no. 4, pp. 1590–1608, 2017.
- [32] K. Singh, S. Biswas, T. Ratnarajah, and F. A. Khan, "Transceiver design and power allocation for full-duplex MIMO communication systems with spectrum sharing radar," *IEEE Trans. Cogn. Commun. Netw.*, vol. 4, no. 3, pp. 556–566, 2018.
- [33] S. Sun, W. U. Bajwa, and A. P. Petropulu, "MIMO-MC radar: A MIMO radar approach based on matrix completion," *IEEE Trans. Aerosp. Electron. Syst.*, vol. 51, no. 3, pp. 1839–1852, Jul. 2015.
- [34] M. Richards, W. Holm, and J. Scheer, *Principles of Modern Radar: Basic Principles*. Raleigh, NC: SciTech Publishin, Inc., 2010.
- [35] M. Radmar, S. M. Karbasi, and M. M. Nayebi, "Data fusion in MIMO DVB-T-based passive coherent location," *IEEE Trans. Aerosp. Electron. Syst.*, vol. 49, no. 3, pp. 1725–1737, 2013.
- [36] D. Gesbert, M. Kountouris, R. W. Heath, C. Chae, and T. Salzer, "Shifting the MIMO paradigm," *IEEE Signal Process. Mag.*, vol. 24, no. 5, pp. 36–46, 2007.
- [37] P. Kumari, J. Choi, N. Gonzalez-Prelcic, and R. W. Heath, "IEEE 802.11ad-based radar: An approach to joint vehicular communication-radar system," *IEEE Trans. Veh. Technol.*, vol. 67, no. 4, pp. 2168–2181, Apr. 2018.
- [38] Q. Shi, M. Razaviyayn, Z. Luo, and C. He, "An iteratively weighted MMSE approach to distributed sum-utility maximization for a MIMO interfering broadcast channel," *IEEE Trans. Signal Process.*, vol. 59, no. 9, pp. 4331–4340, 2011.
- [39] M. R. Bell, "Information theory and radar waveform design," *IEEE Trans. Inf. Theory*, vol. 39, no. 5, pp. 1578–1597, 1993.
- [40] T. M. Cover and J. A. Thomas, *Elements of information theory*, 2nd ed. John Wiley & Sons, 2006.
- [41] J. Liu and M. Saquib, "Transmission design for a joint MIMO radar and MU-MIMO downlink communication system," in *IEEE Global Conf. Signal Info. Process.*, 2018, pp. 196–200.
- [42] Wei Yu and R. Lui, "Dual methods for nonconvex spectrum optimization of multicarrier systems," *IEEE Trans. Commun.*, vol. 54, no. 7, pp. 1310–1322, 2006.
- [43] A. Beck and L. Tetrushvili, "On the convergence of block coordinate descent type methods," *SIAM J. Optim.*, vol. 23, no. 4, pp. 2037–2060, 2013.
- [44] J. Liu and M. Saquib, "Joint transmit-receive beamspace design for colocated MIMO radar in the presence of deliberate jammers," in *Asilomar Conf. Signals Syst. Comput.*, Oct. 2017, pp. 1152–1156.
- [45] C. Chen, M. Li, X. Liu, and Y. Ye, "Extended ADMM and BCD for nonseparable convex minimization models with quadratic coupling terms: convergence analysis and insights," *Math. Program.*, vol. 173, pp. 37–77, 2019.
- [46] Z. Zhang and M. Brand, "Convergent block coordinate descent for training Tikhonov regularized deep neural networks," in *Advances Neural Inf. Process. Syst.*, 2017, pp. 1721–1730.
- [47] Z. Zhu and X. Li, "Convergence analysis of alternating projection method for nonconvex sets," *arXiv preprint arXiv:1802.03889v2*, 2019.
- [48] J. A. Tropp, I. S. Dhillon, R. W. Heath, and T. Strohmer, "Designing structured tight frames via an alternating projection method," *IEEE Trans. Inf. Theory*, vol. 51, no. 1, pp. 88–209, 2005.
- [49] K. B. Petersen and M. S. Pedersen, "The matrix cookbook," nov 2012.
- [50] S. Boyd and L. Vandenberghe, *Convex Optimization*. New York, NY: Cambridge University Press, 2004.
- [51] S. M. Kay, *Fundamentals of statistical signal processing Volume II: Detection theory*. Prentice-Hall, 1993.
- [52] A. Hjørungnes, *Complex-valued matrix derivatives: With applications in signal processing and communications*. Cambridge Univ. Press, 2011.